# Deciphering temporal order of epigenetic changes during lymphomagenesis


A thesis submitted towards partial fulfillment of

BS-MS Dual Degree programme by

**Gaurav Shrikant Joshi**

20141112

IISER Pune

Project Supervisor

**Dr. Holger Bierhoff**

Junior Research Group “Epigenetics of Aging”

Center for Molecular Biomedicine, Department of Biochemistry

Friedrich Schiller University, Jena

## Certificate

This is to certify that this dissertation entitled “Deciphering temporal order of epigenetic changes during lymphomagenesis” towards the partial fulfilment of the BS-MS Dual Degree programme at the Indian Institute of Science Education and Research, Pune represents original work carried out by Gaurav Shrikant Joshi at Center for Molecular Biomedicine (CMB) under the supervision of Dr.Holger Bierhoff, Junior Group leader, Department of Biochemistry, Friedrich Schiller University, Jena during the academic year 2018-19.

**Dr.Holger Bierhoff**

**Junior Group Leader**

**Department of Biochemistry**

**Center for Molecular Biomedicine**

**Friedrich Schiller University, Jena**

**Gaurav Shrikant Joshi**

**BS-MS Student**

**20141112**

**IISER Pune**

**Date: 20th March 2019**

## Declaration

I, Gaurav Shrikant Joshi, hereby declare that the matter embodied in the report entitled "Deciphering temporal order of epigenetic changes during lymphomagenesis" are the results of the work carried out by me at the Center for Molecular Biomedicine (CMB), Department of Biochemistry, Friedrich Schiller University, Jena under the supervision of Dr.Holger Bierhoff and the same has not been submitted elsewhere for any other degree.

**Dr.Holger Bierhoff**

**Junior Group Leader**

**Department of Biochemistry**

**Center for Molecular Biomedicine**

**Friedrich Schiller University, Jena**

**Gaurav Shrikant Joshi**

**BS-MS Student**

**20141112**

**IISER Pune**

**Date: 20th March 2019**

## Abstract

Tumorigenesis is a multistep process with normal cells transitioning through an intermediate pre-tumor stage to eventually transform into tumor cells. However, the underlying temporal order of epigenetic changes in these intermediate stages of tumorigenesis is poorly studied. Using the Eμ-Myc mice model of spontaneous B-cell lymphoma, we have dissected into the transcription and DNA methylation changes specifically from the bivalent genes and the ribosomal DNA (rDNA) locus during lymphomagenesis. We report an increase in rDNA transcription with a counterintuitive increased fraction of promoter-methylated rDNA repeats during tumorigenesis. We propose that the increased promoter methylation safeguards a fraction of rDNA repeats from transcription induced damage and promotes cancer cell survival. We report peculiar patterns of gene expression changes in epigenetic modifiers at different stages of tumorigenesis. We also report a characteristic transient increase in the expression of developmental genes from the bivalent promoters despite increased DNA methylation in the early pre-tumor stage of tumorigenesis. Taken together, the novel findings from our study give us interesting insights into the temporal order of epigenetic changes during tumorigenesis.

# Index

# List of Figure and Tables

## Acknowledgement

I express my sincere gratitude to my thesis advisor, Dr.Holger Bierhoff, Junior Group Leader, CMB, Jena for his valuable guidance and support throughout my thesis. I would also like to thank him for providing me with all the resources and encouragement to test my ideas during the study. I would like to thank Dr.Christian Kosan and Dr.Rene Winkler for their guidance and help with the mouse model. I would also like to thank the FLI Core Facility for their help in sequencing and FACS. I would like to thank our bioinformatics collaborators from Leibniz Institute on Aging, Jena, Dr.Steve Hoffmann and Konstantin Riege for their help in analyzing the sequencing data. I would also like to thank all the members of the Bierhoff group and the biochemistry department at CMB for providing me with a friendly and motivating work environment.

I would also take this opportunity to thank my family and friends for their constant help and support. It is their support that has always propelled me further to pursue scientific research.

I would also like to thank all my past project advisors during different internships, Dr.Saikrishnan Kayarat (IISER Pune), Dr.Partho Sarothi Ray (IISER Kolkata), Dr.Kundan Sengupta (IISER Pune) and Dr.Karl Lenhard Rudolph (FLI, Jena) for motivating me and inculcating important research ethics in me over the past years.

Finally, I thank IISER Pune for providing excellent teaching and research facilities as well as exposure to science during the complete course of BS-MS degree.

# 6. Introduction

## 6.1. Cancer

Cancer is inevitably linked with uncontrolled cell division and proliferation. Multiple theories have been proposed for cancer origins and progression back from 1954 involving DNA mutations (Armitage and Doll, 1954), followed with the classic two-hit model in retinoblastoma (Knudson, 1971) and few recent theories based on epigenetic alterations (Baylin and Jones, 2016) and cellular selection (Greaves, 2007). The hallmarks of cancer cells including the ability to resist cell death, metastatic signaling, replicative immortality, etc are reviewed thoroughly by D.Hanahan and R.Weinberg (Hanahan and Weinberg, 2011). Over the last decade, the use of modern next-generation sequencing tools has revealed the presence of hierarchy and heterogeneous cell populations in a tumor mass (Levitin et al., 2018). Therefore, nowadays tumor is considered more of a multicellular ecosystem which extensively interacts with its microenvironment (Balkwill et al., 2012) and the immune system (Wellenstein and de Visser, 2018).

Normal cells gain tumorigenic potential mainly from genetic and epigenetic alterations. The genetic alterations include DNA mutations, chromosomal aneuploidy and gene copy number changes (Wong et al., 2011). The common effect of such genetic alterations is the increased expression of oncogenes (e.g., MYC, KRAS, EGFR), silencing of tumor suppressor genes (e.g., TP53, BRAC1, PTEN) or rendering the tumor suppressor proteins functionally inactive (Bailey et al., 2018). However, in this work we have moved beyond the genetic aspects and dissected the role of epigenetics in tumorigenesis.

## 6.2. Epigenetics

The study of dynamic, reversible and heritable mechanisms regulating gene expression, without affecting the underlying DNA sequence, fall within the purview of epigenetics. The three major epigenetic mechanisms of gene regulation are post-translational histone modifications (Suganuma and Workman, 2011), DNA methylation (Cedar and Bergman, 2012) and non-coding RNAs (ncRNAs) (Meller et al., 2015).

The developmental pathways and cell fate decisions are regulated by these epigenetic mechanisms to heritably maintain cell type-specific gene expression patterns (Reik, 2007). Deregulation in post-translational histone modifications (Audia

and Campbell, 2016), DNA methylation (Kulis and Esteller, 2010) and expression of ncRNAs (Lin and He, 2017) lead to aberrant gene expression patterns associated with tumorigenesis.

### 6.2.1. DNA methylation

In eukaryotes, DNA is methylated at the 5' position of cytosine (5mC) by DNA methyltransferases (DNMTs). The DNMT family includes DNMT1, DNMT2 and DNMT3 (DNMT3a, DNMT3b, DNMT3c and DNMT3l) (Goll and Bestor, 2005). The DNMT1 maintains DNA methylation patterns during cell division by acting on hemimethylated DNA (Easwaran et al., 2004). DNMT3a and DNMT3b are *de novo* DNA methyltransferases regulating genome-wide methylation (Chédin, 2011). The 5mC DNA modification is erased by the Ten Eleven Translocation (TET) family of methylcytosine dioxygenases (Wu and Zhang, 2011).

DNA methylation is abundantly present at the repetitive elements in the genome and is also proposed to have evolved as a suppressor of transcription from these repetitive elements (Yoder et al., 1997). DNA methylation is also found at the CG dinucleotide rich regions called CpG islands, present in most gene promoters. Conventionally, promoter DNA methylation is thought to inhibit transcription factor binding leading to transcription inhibition (Weber et al., 2007). However, a recent study of human transcription factors reported homeodomain-containing transcription factors to have higher binding efficiency to methylated DNA (Yin et al., 2017). Gene body methylation inhibits spurious intragenic transcription initiation and promotes transcriptional elongation (Neri et al., 2017).

Whole Genome Bisulfite Sequencing (WGBS) and methyl-DNA Immunoprecipitation (me-DIP) are used to map the 5mC sites in the genome. These techniques revealed that cancer cells show genome-wide hypomethylation, predominantly at the repetitive elements (Ehrlich, 2002) and hypermethylation at CpG islands (Sproul and Meehan, 2013). The hypomethylation at the repetitive elements leads to activation of transposons, leading to genomic instability which is a hallmark of cancer (Hanahan and Weinberg, 2011). This altered distribution of DNA methylation in cancer is attributed to mutations or overexpression of DNMTs and TET proteins (Huang and Rao, 2014; Zhang and Xu, 2017).

### 6.2.2 Frequently Bivalent Segments (FBS)

In eukaryotes, ~147 bp DNA is wrapped around core histones (H2A, H2B, H3 and H4) to form the nucleosome particle (Luger et al., 1997). The amino acids in the N-terminal tails of the core histones undergo post-translational modifications such as methylation (me), acetylation (ac), phosphorylation (ph), etc (Zhao and Garcia, 2015). The histone modifications modulate gene transcription while the modification themselves are under the control of histone “writer” and “eraser” proteins (Zhao and Garcia, 2015). The altered distribution of histone modifications in cancer is associated with transcriptional deregulation of oncogenes and tumor suppressor genes (Audia and Campbell, 2016). DNA methylation and histone modifications feedback to each other to modulate transcription (Du et al., 2015). Methyl-CpG-binding domain (MBD) proteins act as a platform for the recruitment of transcription repression complexes such as HDACs, Sin3A, HP1, etc (Bogdanović and Veenstra, 2009).

Bivalent regions are the genomic locations with both activating (predominantly H3K4me1 and H3K4me3) and repressive (predominantly H3K27me3) histone modifications present simultaneously (Bernstein et al., 2006). Such bivalent regions are found in the majority of developmental gene promoters in both stem cells and differentiated cells (Mikkelsen et al., 2007). The genes with bivalent promoters are transcriptionally silent but have poised RNA polymerase II for rapid transcriptional activation upon receiving differentiation signals. Embryonic stem cells during differentiation lose either the activatory or the repressive histone modification depending on the transcriptional requirements of differentiated cells. That being said, not all bivalent regions are lost during differentiation, but differentiated cells possess them at lesser genomic locations when compared with stem cells (Bernstein et al., 2006).

A recent study mapped the locations of frequently bivalent chromatin segments (FBS) which are common to more than 80% human cell types including embryonic stem cells (ESCs), induced pluripotent stem cells (iPSCs) and differentiated cells (Bernhart et al., 2016). These FBS as expected are associated with developmental gene promoters and were shown to become significantly unstable in cancer cells (Fig 1a). The bivalent regions are maintained in an unmethylated state in normal cells but interestingly become hypermethylated in cancer cells (Bernhart et al., 2016; Rodriguez et al., 2008; Veland et al., 2019). Despite the hypermethylation, FBS associated developmental genes showed a counterintuitive increase in gene expression (Fig 1b).

The underlying mechanisms for the instability of bivalent regions and the associated transcriptional deregulation in cancer cells remain unclear. The Bernhart et al. study reported these changes by comparing normal and tumor cells as the information on epigenetic changes at the frequently bivalent regions in the intermediate pre-tumor stage of most cancers is missing.

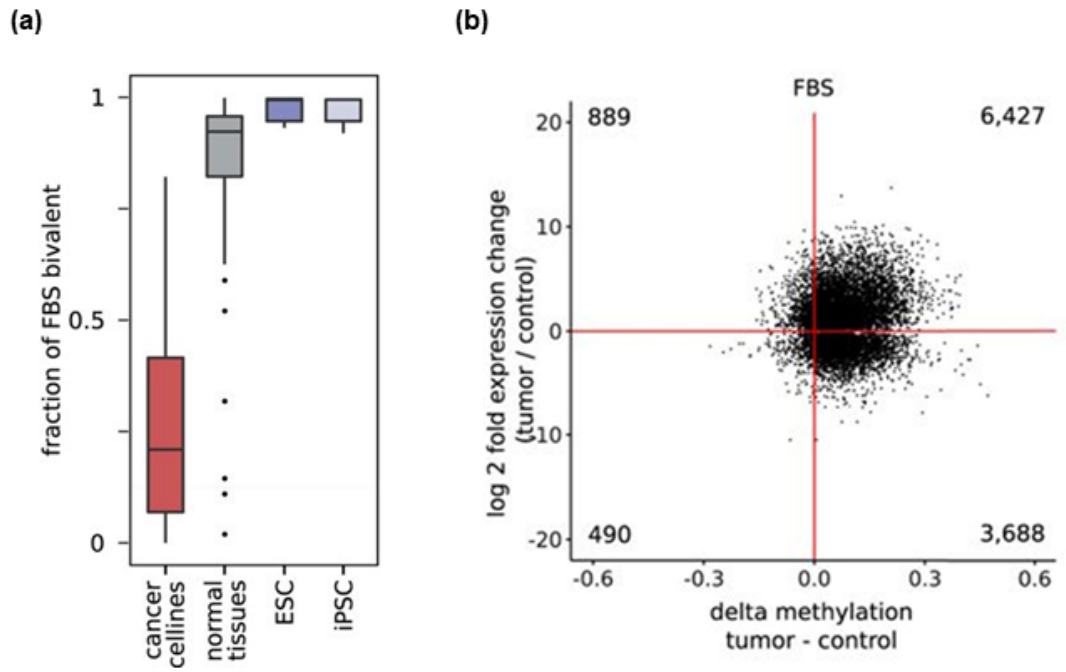


**Figure 1 : Changes in FBS during tumorigenesis (Adapted from Bernhart et al., 2016).**

**(a)** The plot shows the changes in fraction of FBS which remain bivalent in cancer cell lines, normal tissues, embryonic stem cells (ESC) and induced pluripotent stem cells (iPSCs). Cancer cell lines can be seen to have a strikingly reduced fraction of bivalent regions compared to normal tissues, ESCs and iPSCs.

**(b)** The scatter plot shows the change in DNA methylation (X-axis) and the $\log_2$-fold change in gene expression (Y-axis) from FBS associated genes. The numbers in the corner of each quadrant represent the number of genes in that respective quadrant.

### 6.3. Ribosomal DNA (rDNA) transcription regulation

In eukaryotes, genes encoding ribosomal RNA (rRNA) are present in multiple copies and are located inside the nucleolus. In humans and mice, RNA Polymerase I (RNA Pol I) transcribes rDNA into a precursor RNA (pre-rRNA), which is then processed into 5.8S, 18S and 28S rRNAs (Mullineux and Lafontaine, 2012). The pre-initiation complex required for initiating transcription of rDNA consists of upstream

binding factor (UBF), selective factor 1 (SL1) and transcription initiation factor IA (TIF-IA) (Fig 2a). Once the PIC is established, TIF-IA undergoes post-translational modifications and recruits RNA Pol I, to initiate transcription (Yuan et al., 2002). The assembly of PIC and transcription initiation is regulated by post-translational modification of UBF and TIF-IA via growth and stress signaling pathways (e.g. mTOR, MAPK) and epigenetic modifications in the form of promoter DNA methylation and histone modifications (Santoro and Grummt, 2001; reviewed in Sharifi and Bierhoff, 2018). The actively transcribed rDNA repeats have H3K4me3, H3K36me3, H2AQ104me, etc histone marks and the promoter DNA is unmethylated. On the other hand, silent rDNA repeats have H3K27me3, H3K9me3, H4K20me3, etc histone marks and the promoter DNA methylated (Fig 2b) (reviewed in Sharifi and Bierhoff, 2018).

Under normal conditions, a fraction of the rRNA genes are maintained in a transcriptionally repressed state. The nucleolar remodeling complex (NoRC), consisting of TIP5 and SNF2H along with the promoter RNA (pRNA), acts as a platform for recruitment of histone modifiers and DNMTs to silence rRNA genes (Strohner et al., 2001; Bierhoff et al., 2010). NoRC-mediated methylation of the rDNA promoter is crucial for constitutive silencing, which can be pinpointed in mice to methylation of the cytosine at position -133 upstream of transcription start site (Santoro and Grummt, 2001). In addition, the transcription-permissive rRNA genes are also regulated by multiple epigenetic mechanisms, indicating that they can be affected by cancer-associated epimutations. In fact, cancer cells show transcriptional upregulation of pre-rRNA, enlarged nucleoli and increased ribosome biogenesis, which supports the rapid proliferation rates in cancer cells (Pelletier et al., 2018). However, the characterization of the temporal order of epigenetic changes regulating rDNA transcription during tumorigenesis remains limited.

The strong dependence of cancer cells on ribosome biogenesis makes rDNA transcription regulation a promising avenue in therapy. Many clinically applied cancer drugs indeed have inhibition of rDNA transcription or processing in their spectrum of action (Derenzini et al., 2018). Moreover, a highly specific inhibitor of RNA Pol I, CX-5461, is currently in Phase I/II clinical trials for the treatment of hematologic malignancies and triple negative breast cancer (Drygin et al., 2011; Devlin et al. 2016).

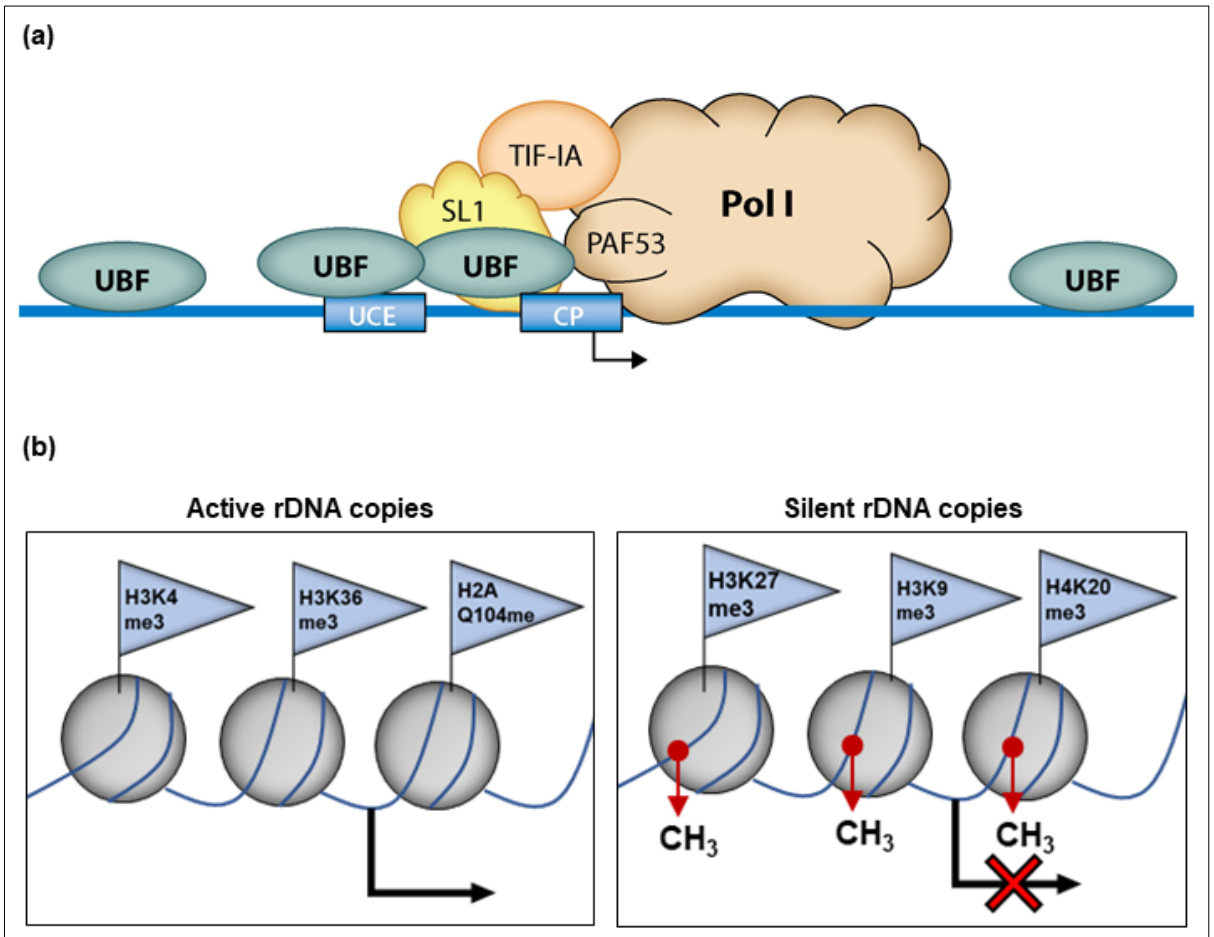


**Figure 2 : Regulation of rDNA transcription.**

**(a)** The schematic shows the components of RNA Pol I pre-initiation complex required for rDNA transcription and pre-rRNA synthesis. Adapted from Sharifi and Bierhoff, 2018.

**(b)** The schematic represents the set of histone modifications and DNA methylation marks demarcating the active and silent rDNA copies.

## 6.4. Experimental plan

The characterization of epigenetic changes in tumorigenesis is mainly performed either in cancer cells or primary tumor samples. Cultured cancer cells are a convenient working model for cancer but lack crucial tumor microenvironment interactions and undergo genetic and epigenetic changes due to culturing (Balkwill et al., 2012). On the other hand, primary tumor samples consist of a heterogeneous population of cells in different states of tumorigenesis (Levitin et al., 2018). Therefore, these studies provide an averaged view of epigenetic changes occurring during tumorigenesis. In this study, we have primarily focused on characterizing transcription and DNA methylation changes both at genome-wide (bivalent genes) and gene-specific context (rDNA) during tumorigenesis.

To investigate the temporal order of epigenetic and gene expression changes during tumorigenesis, we have employed the Eμ-Myc mouse model of spontaneous B-cell lymphoma in our study (Harris et al., 1988). This system is akin to the human Burkitt's lymphoma by having a c-Myc transgene under the control of an IgH enhancer which leads to Myc overexpression specifically in the B-cell lineage. Thus, we could compare B-cells from wild-type mice and Eμ-myc in either a pre-tumor or a tumor state. Moreover, by flow cytometric separation of pre-tumor B-cells in benign (wild-type like) and transformed (tumor-like) subpopulations, we achieved a high temporal resolution of progressive changes in cancer formation. We performed RNA-seq and WGBS to analyze for transcriptomic and DNA methylation changes respectively, in each successive stage of tumorigenesis (wild-type, pre-tumor and tumor) (Fig 3a).

We used this sequencing dataset towards the identification of early and late epigenetic drivers and networks of transcription factors regulating tumorigenesis. We also used this dataset to investigate further the aforementioned counterintuitive positive correlation between DNA methylation and transcription of developmental genes from the FBS, reported for multiple human cancers (Bernhart et al., 2016).

Parallel to this genome-wide approach we specifically investigated epigenetic regulation of rRNA genes during tumorigenesis. High transcriptional activity and the repetitive nature of rDNA makes it prone to recombination and genomic instability (Salim and Gerton, 2019) while the heterochromatic fraction is believed to have a stabilizing function (Srivastava et al., 2016). We have therefore investigated how

aberrant activation of rRNA synthesis during tumorigenesis affects rDNA silencing and integrity.

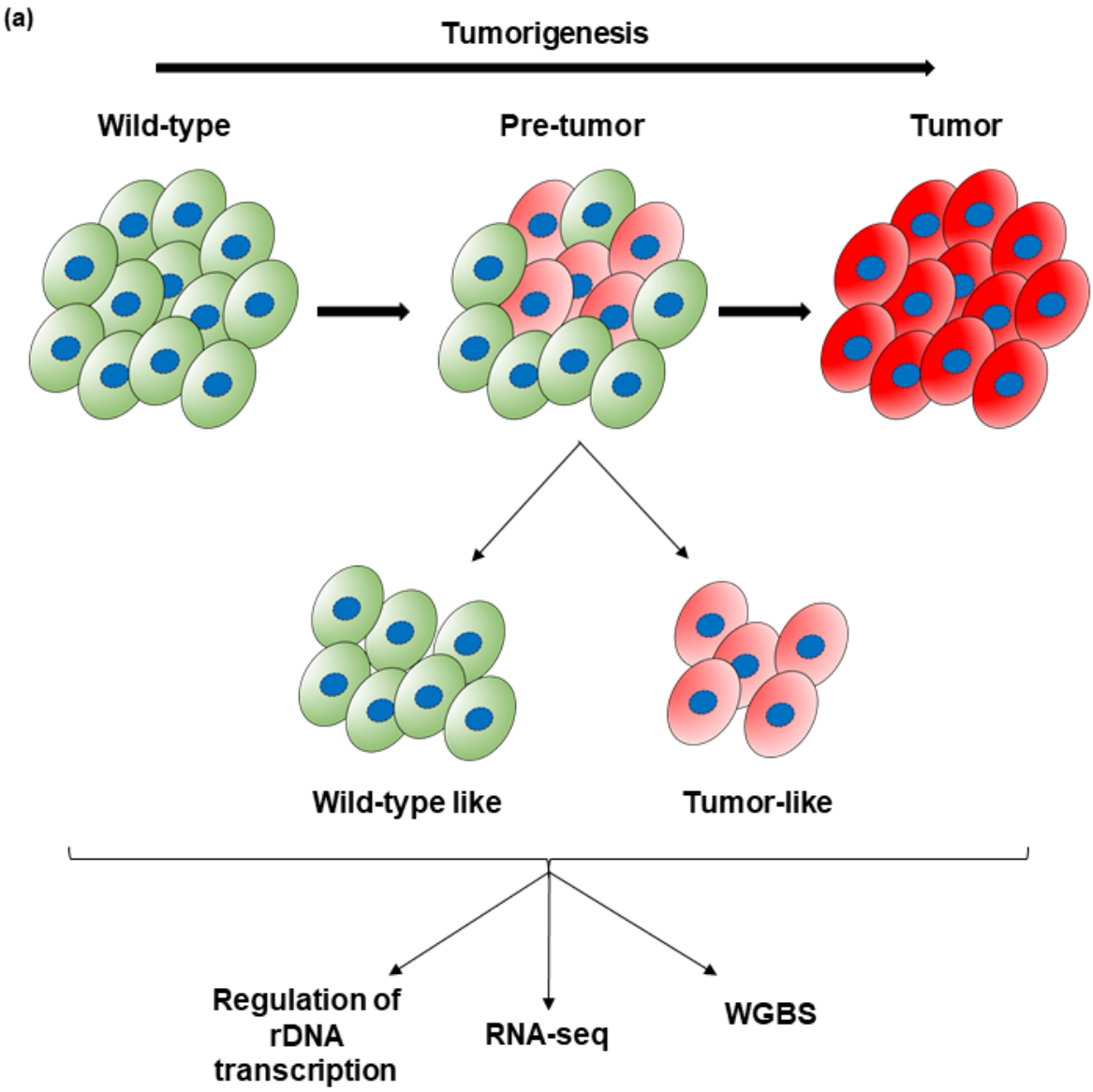


**Figure 3 : Experimental workflow.**

**(a)** The schematic represents different stages of tumorigenesis viz. wild-type, pre-tumor and tumor. It also outlines the experimental plan of this study which includes isolation of unique cell populations during tumorigenesis to analyse the regulation of rDNA transcription and to perform RNA-seq and WGBS.

# 7. Materials and Methods

## 7.1. Eμ-Myc mice and B-cell isolation

The mice used in the study were from C57BL/6 background, with the Eμ-Myc mice maintained in a heterozygous state. Wild-type and pre-malignant mice were sacrificed at age 8-10 weeks while malignant mice were sacrificed as soon as they developed lymphoma, which was usually at age 10-12 weeks. B-cells were isolated from spleen of wild-type and pre-malignant Eμ-Myc mice, while the tumor B-cells were isolated from lymph nodes of Eμ-Myc mice. The isolated B-cells were not cultured but directly processed for experiments.

## 7.2. Fluorescence-activated cell sorting (FACS)

Freshly isolated spleen or lymph nodes were crushed in Phosphate Buffer Saline (PBS) (Sigma, D8537) using slides to liberate the cells into suspension. The cells were spun down at 700xg for 5 min and incubated with hypotonic red cell lysis buffer (155mM $NH_4Cl$, 12mM $NaHCO_3$, 0.1mM EDTA) for 10 min at room temperature. The red cell lysis was stopped by adding PBS and cells were spun down again. The cells were then stained with fluorescent antibodies for 15 min at 4°C and washed twice with PBS before sorting.

Fluorescent antibodies used in FACS: anti-CD19-FITC (Biolegend, 101505), anti-B220-APC (eBioscience, 17-0452-83) and anti-IgM-PE-Cy7 (eBioscience, 25-5890-83). Wild-type B-cells were gated as single live CD19+ / B220+ cells. The pre-tumor B-cells were pre-gated on CD19 and separated into two populations based on surface levels of B220, named henceforth pre-tumor high and pre-tumor low. The tumor cells were specifically enriched in the lymph nodes hence required no further sorting. The purity of isolated tumor cells was tested by staining a fraction of isolated cells with anti-CD19-FITC, anti-B220-APC and anti-IgM-PE-Cy7 antibodies. Tumor cell isolations which have CD19+ / B220 low / IgM− cells with purity of ~95% were used in this study.

## 7.3. Cell culture

NIH3T3 mouse fibroblast cells obtained from ATCC and the ecotropic packaging cell line Phoenix obtained from Nolan lab were maintained in DMEM high glucose medium (Sigma, D0819) supplemented with 10% FBS (Not of USA origin,

Sigma-Aldrich), 90U/mL penicillin and 90µg/mL streptomycin antibiotics (PAA) at 37°C, 5% CO2. The cells were split at regular intervals using Trypsin-EDTA (Sigma, T3924).

### 7.4. Transfection and transduction

Phoenix cells were transfected with pBabe-Myc-puro by the calcium phosphate method. The transfection mix contained 20µg of pBabe-Myc-puro plasmid, 50µL of 2.5M $CaCl_2$ and millipore $H_2O$ to make up the volume upto 500µL. To this mix, 500µL of 2x HEPES buffered saline (HBS, 50mM HEPES, 280mM NaCl) was added with continuous vortexing. The transfection mix was incubated at room temperature for 10 min before adding to cells.

Virus containing medium was collected after 36 h of infection. NIH3T3 cells (0.5 million per 10 cm dish) were seeded a day before transduction. 6mL virus containing medium was filtered using the 0.45µm filter and added to NIH3T3 cells with 10µg/mL polybrene for 8 h. Transduced cells were selected using 7µg/mL puromycin for 48 h.

### 7.5. Protein extraction

Cultured cells were washed twice in ice-cold PBS and scrapped in 1mL ice-cold PBS. The cells were centrifuged for 5 min at 2000 rpm at 4°C and cell pellet was resuspended in 1mL ice-cold protein lysis buffer (2x Tris-buffered saline (TBS), 1% v/v Triton X-100, 2mM EDTA, 0.1% w/v SDS, 1x Protease inhibitor cocktail). The cells were incubated with the lysis buffer for 1 h at 4°C. The cell debris were cleared by centrifuging at 12000 rpm for 15 min at 4°C. The protein containing supernatant was stored at -20°C. Protein quantification was performed using standard Bradford reagent (Sigma-Aldrich, B6916) and measuring the absorbance at 595 nm.

### 7.6. SDS-Polyacrylamide Gel Electrophoresis (SDS-PAGE)

Proteins were separated on a 12% polyacrylamide gel. The stacking gel (5% v/v Acrylamide, 125mM Tris-HCl [pH 6.8], 0.1% w/v SDS, 0.1% w/v APS, 0.0001% w/v TEMED) and separating gel (5% v/v Acrylamide, 125mM Tris-HCl [pH 8.8], 0.1% w/v SDS, 0.1% w/v APS, 0.0001% w/v TEMED) were casted in the gel casting apparatus with 1.5mm spacer. 20µg of protein in 20µL was added to 10µL 3x laemmli buffer. The samples were heat denatured for 10 min at 95°C. 5µL of PageRuler Plus prestained protein ladder (Thermo Scientific, 26619) and the denatured protein

samples were loaded on the gel. The electrophoresis run was performed in a Mini-PROTEAN Tetra System with 1x running buffer (25mM Tris-HCl, 190mM Glycine, 0.1% w/v SDS) at 100 V until the dye front reached the separating gel. The voltage was then increased to 120 V.

### 7.7. Western Blot

Western blot was performed using a semi-dry approach on the Trans-Blot Turbo Transfer System. Filter papers and nitrocellulose transfer membrane (Roth, Roti-NC 0.45) were briefly wetted in transfer buffer (25mM Tris-HCl, 200mM Glycine, 20% v/v Methanol). The polyacrylamide gel was then stacked along with the transfer membrane between filter papers. The transfer was carried out at 25 V for 35 min. The transfer membrane was blocked using 5% milk in TBST (1x TBS and 0.1% Tween-20) for 1 h at room temperature. The membrane was incubated with anti-c-Myc (Santa Cruz, N-262, 1:1000 dilution) and anti-tubulin (Sigma-Aldrich, A2066, 1:2000 dilution) primary antibody prepared in 5% milk in TBST, overnight at 4°C. The next day, membrane was washed four times in TBST for 10 min each. The membrane was then incubated with secondary anti-rabbit-IgG HRP antibody (Dianova GmbH, dilution 1:5000) prepared in 5% milk in TBST for 1 h at room temperature. The membrane was washed again four times for 10 min each with TBST. After the last washing step, 1mL of SuperSignal West Pico Plus chemiluminescent substrate (Thermo Scientific, 34580) was added to the membrane and the membrane was visualized using the Vilber Lourmat Fusion Solo S system.

The fold change in Myc protein levels was quantified using integrated density values of the Myc protein band in control and Myc overexpressing cells using ImageJ Fiji software. Integrated density values of tubulin were used as a normalization control.

### 7.8. RNA extraction

Cells were lysed in 1mL TriFast reagent (VWR, 30-2010). RNA used for RNA-seq was isolated using Direct-zol RNA kit (Zymo research, R2060) as per the manufacturer's instructions. In brief, 1mL of 100% ethanol was added to TriFast lysed cells, wash followed with on-column DNase I digestion, wash followed with elution of RNA in nuclease-free water.

RNA extraction from cell lines was performed using isopropanol precipitation method. 200µL of 1-Bromo-3-chloropropane (BCP) (Sigma, B9673) was added per

1mL of TriFast lysed cells. The samples were briefly vortexed and centrifuged at 12000xg for 15 min at 4°C. The aqueous phase was taken out carefully and equal volume of isopropanol (Roth) was added. The samples were kept at RT for 15 min for the RNA to precipitate. The samples were centrifuged at 12000xg for 15 min at 4°C. The RNA pellet was washed twice with 1mL 70% ethanol. The RNA pellet was air-dried and resuspended in DEPC (Diethyl pyrocarbonate) treated water. The RNA samples were stored at -80°C until further use.

### 7.9. Genomic DNA extraction

Genomic DNA (gDNA) used for Whole Genome Bisulfite Sequencing was isolated using Quick-DNA miniprep kit (Zymo research, D4074) as per the manufacturer's instructions. In brief, the cells were lysed and treated with Proteinase K and RNase A to degrade proteins and RNA respectively. The lysate was then loaded on column, washed and column bound gDNA was eluted in nuclease-free water.

gDNA extraction from the cell lines was performed using the Blood DNA extraction kit (Qiagen, 51104) as per the manufacturer's instructions. The isolated gDNA was checked for any shearing during isolation by running it on 0.8% agarose gel.

### 7.10. Polymerase Chain Reaction (PCR)

The PCR constituted of 3µL template DNA, 3µL 5x GoTaq Buffer, 1µL 1.5mM MgCl2, 1µL DMSO, 0.3µL 10µM dNTPs, 0.5µL 10µM primer mix (forward and reverse primers), 0.1µL 5U/µL GoTaq polymerase (Promega, M3001) and the volume was made up to 15µL with millipore $H_2O$. The thermocycler conditions were 95°C for 2 min, followed by 30 cycles of 95°C for 30 sec, 60°C for 30 sec, 72°C for 30 sec, followed by 72°C for 5 min.

### 7.11. cDNA synthesis

2µg of RNA was treated with DNase I (Sigma, AMPD1) to degrade any residual gDNA. The 10µL reaction was setup with 1µL 10x DNase digestion buffer, 1µL DNase I and 8µL RNA sample. The reaction was incubated at 37°C for 30 min, stopped by adding 1µL stop solution and incubating at 65°C for 10 min.

The cDNA synthesis was performed using SuperScript IV (SSIV) First-Strand Synthesis System (Thermo Fisher, 18091050). Reaction mix containing DNase I

digested RNA (upto 5.5µL), 0.5µL 50µM random hexamers and 0.5µL 10mM dNTPs was denatured at 65°C for 5 min and quick chilled. To this mix, 2µL 5x SSIV buffer, 0.5µL 0.1M DTT, 0.5µL RiboLock (Thermo Fisher Scientific, EO0381) and 0.3µL Reverse Transcriptase enzyme was added. For every RNA sample, a control reaction without Reverse Transcriptase (−RT) was setup. The −RT samples were then subjected to PCR using primers amplifying the 18S rDNA region to test for gDNA contamination.

### 7.12. Quantitative PCR (qPCR)

The 10µL qPCR reaction constituted of 5µL 2x Maxima SYBR Green/ROX qPCR Master Mix (Thermo Fisher, K0221), 0.25µL 10µM primer mix (forward and reverse primers), 1.75µL millipore $H_2O$ and 3µL diluted cDNA. For pre-rRNA and B2M quantification, cDNA was diluted 1:50.

The protocol has an initial step of 95°C for 10 min, followed by 45 cycles of 95°C for 15 sec and 60°C for 60 sec. A DNA dilution series was included to quantify the primer efficiency using standard curve. The primer efficiency was then used to transform the $C_t$ values into quantity by the Applied Biosystem QuantStudio 3 Real-Time PCR System Software.

### 7.13. Primer sequences

| Primer name | Sequence (5'--> 3') |
|---|---|
| mrDNA -127/-105 for | TGGGGTCATTTTTGGGCCACC |
| mrDNA -205/-185 for | GACCTGTCGGTCTTATCAGTTC |
| mrDNA -21/-1 rev | ACCTATCTCCAGGTCCAATAG |
| mm_gene desert for | AGGGACCTGACTGGTGACTG |
| mm_gene desert rev | GTCCTGTCTGCATCCCATTT |
| mm_pre-rRNA for | CGTGTAAGACATTCCTATCTCG |
| mm_pre-rRNA rev | GCCCGCTGGCAGAACGAGAAG |
| mm_B2M for | CTGCTACGTAACACAGTTCCACCC |
| mm_B2M rev | CATGATGCTTGATCACATGTCTCG |

### 7.14. CHOP-qPCR assay for 5mC quantification

In mice, rDNA transcription is inhibited by methylation at the -133 position cytosine (Santoro and Grummt, 2001). HpaII is a methylation sensitive while MspI is a methylation insensitive restriction enzyme both recognizing CCGG sequence. This restriction site is present at the -143 position in rDNA promoter whose methylation correlates with the methylation of -133 site. The restriction digestion reaction comprised of 100ng gDNA (upto 8µL), 1µL 10x CutSmart buffer and 1µL HpaII (NEB, R0171S) or MspI (NEB, R0106S) restriction enzyme. The restriction digestion reaction was kept at 37°C for 1 h followed with enzyme inactivation at 80°C for 20 min. Flanking primer pair mrDNA -205/-185→mrDNA -21/-1 was used to quantify the amount of HpaII resistant DNA by qPCR. The normalization for input gDNA was performed using a primer pair mrDNA -127/-105→mrDNA -21/-1 amplifying region downstream of the

restriction site. Amplicon -205/-1 was normalized to -127/-1 to calculate the fraction of promoter-methylated rDNA repeats.

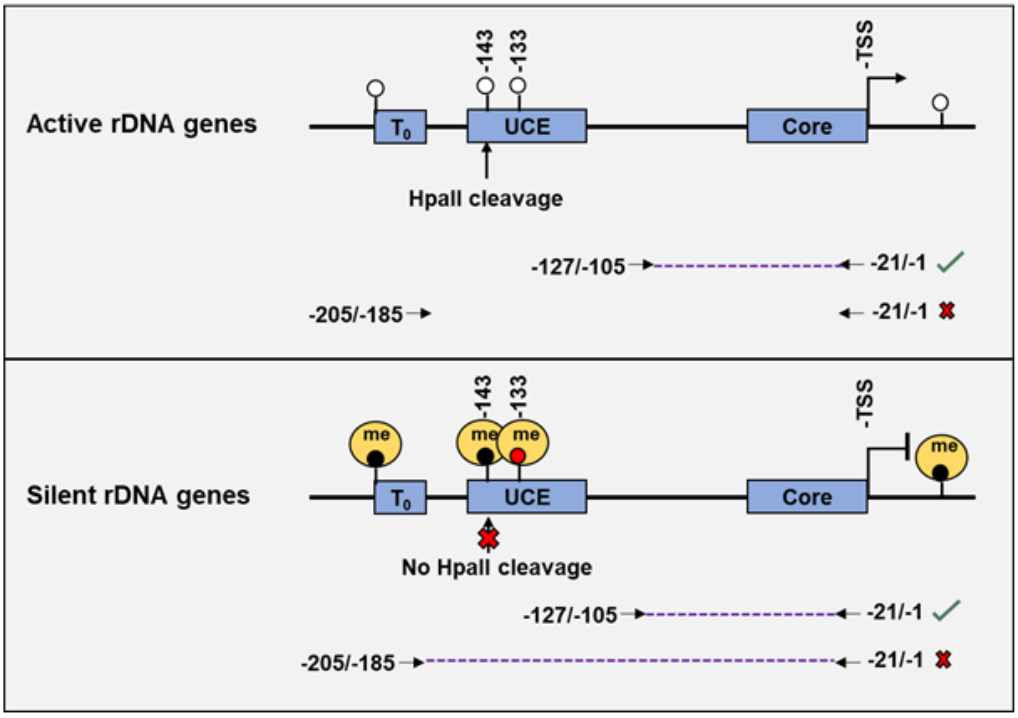


**Figure 4 : CHOP-qPCR assay.**

**(a)** The schematic represents the CHOP-qPCR assay used in the study to quantify fraction of promoter methylated rDNA repeats. Modified from McStay and Grummt (2008).

## 7.15. 5-hydroxy-methylcytosine (5-hmC) quantification

The 5-hmC levels in the rDNA promoter were measured using Quest 5-hmC Detection Kit (Zymo Research, D5410). The kit has a glucosyltransferase enzyme which leads to glycosylation of 5-hmC. The MspI restriction enzyme is sensitive to glucosylated-5-hmC but cleaves at sites with 5-mC and unmethylated cytosine. 100ng gDNA was used for the detection of 5-hmC. The glycosylation and restriction digestion reaction with MspI was performed as per manufacturer's instructions. The mrDNA -205/-185→mrDNA -21/-1 primer pair was used to quantify MspI resistant DNA, representing the fraction of 5-hmC modified rDNA repeats. While the mrDNA -127/-105→mrDNA -21/-1 primer pair was used for normalization of input DNA in qPCR.

### 7.16. rDNA copy number analysis

The rDNA copy number was quantified relative to a single copy control genomic region using qPCR based approach. 10ng of gDNA was used as template in the qPCR reaction. The primer pair of mrDNA -205/-185 →mrDNA -21/-1, amplifying the rDNA promoter regions was used to quantify the rDNA repeats in the genome. The normalization for the input gDNA was performed using single copy genomic region in the gene desert region on mouse chromosome 15.

### 7.17. Chromatin Immunoprecipitation (ChIP)

Freshly isolated wild-type or tumor B-cells were fixed for 10 min with 1% formaldehyde at room temperature and crosslinking was quenched with 125mM glycine for 5 min. Cells were spun down and washed once with PBS. Nuclei were isolated by successive incubation in lysis buffer A (100mM [pH 8] Tris-HCl, 10mM DTT, 15 min on ice followed with 15 min at 30°C), lysis buffer B (10mM [pH 7.5] HEPES, 10mM EDTA, 0.5mM EGTA, 0.25% Triton X-100, 5 min on ice) and lysis buffer C (10mM [pH 7.5] HEPES, 10mM EDTA, 0.5mM EGTA, 200mM NaCl, 5 min on ice). Nuclei were disrupted in lysis buffer D (50mM [pH 8.0] Tris-HCl, 10mM EDTA, 1% SDS) and chromatin was fragmented using Bioruptor Pico (Diagenode, B01060010) to an average length of 200-500 bp. The sonicated chromatin suspension was spun down at 12000xg for 10 min at 10°C to get rid of cell debris. Chromatin present in the suspension was diluted with 5 volumes of ChIP-buffer (15mM [pH 8.0] Tris-HCl, 180mM NaCl, 1.2mM EDTA, 1.2% Triton X-100). Protein A/G-Sepharose beads (GE Healthcare) were blocked using 0.25mg/mL herring sperm DNA, 1mg/mL BSA and 1% gelatin from cold water fish skin. Chromatin was pre-cleared for 1 h at 4°C using blocked Protein A/G-Sepharose beads. 10% (v/v) input chromatin was taken out and stored at -20°C. Approximately 20µg chromatin was incubated with 1 to 5µg of anti-RPA116 antibody or no antibody as control, overnight at 4°C followed by incubation with blocked Protein A/G-Sepharose beads for 1 h.

The beads were washed two times each in low salt wash buffer (20mM [pH 8.0] Tris-HCl, 150mM NaCl, 2mM EDTA, 0.1% SDS,1% Triton X-100), high salt wash buffer (20mM [pH 8.0] Tris-HCl, 500mM NaCl, 2mM EDTA, 0.1% SDS, 1% Triton X-100), LiCl wash buffer (10mM [pH 8.0] Tris-HCl, 250mM LiCl, 1mM EDTA, 1% sodium deoxycholate, 1% NP-40) and TE buffer (10mM [pH 8.0] Tris-HCl, 2mM EDTA). DNA was eluted from the beads using freshly prepared elution buffer (0.1M NaHCO3, 1%

SDS) by incubating beads three times in 50µL elution buffer for 10 min at room temperature. De-crosslinking was performed by heating the eluted chromatin at 65°C for 6 h followed with DNA purification using ChIP-DNA Clean & Concentrator Kit (Zymo Research, D5201) kit.

### 7.18. Whole Genome Bisulfite Sequencing (WGBS)

The Whole Genome Bisulfite Sequencing libraries were prepared using Pico Methyl-Seq Library Prep Kit (Zymo Research, D5455) as per the manufacturer's instructions. In brief, 10ng of gDNA was used for the library preparation which included bisulfite conversion and library amplification steps. The libraries were then purified using the provided DNA isolation kit. The quality of library was analyzed on Agilent Bioanalyzer 2100 (Agilent) and fragment size was observed between 200-400 bp. Sequencing of these libraries was performed using HiSeq2500 with 100bp paired-end-sequencing in high-output mode. The data extraction was performed using bcl2FastQ v2.19.1.403 software.

### 7.19. RNA-sequencing (RNA-seq)

The RIN value for each RNA sample was measured on Agilent Bioanalyzer 2100 (Agilent Technologies). RNA samples with RIN value greater than 7 were used for library preparation and RNA-seq. 200ng of total RNA was processed through TruSeq Stranded Total RNA Library Prep Kit with Ribo-Zero Gold (Illumina) to deplete rRNAs and generate sequencing libraries. The quality of these libraries was measured on Agilent Bioanalyzer 2100. Libraries were sequenced using HiSeq2500 as 50bp single-end-sequencing with high-output mode. The data extraction was performed using bcl2FastQ v2.19.1.403 software. Approximately, 40-70 million reads were captured per sample.

### 7.20. RNA-seq and WGBS analysis pipeline

The mapping of the RNA-seq and WGBS reads was performed by Konstantin Riege using the following pipeline. The downstream functional analysis of the sequencing data was performed by me.

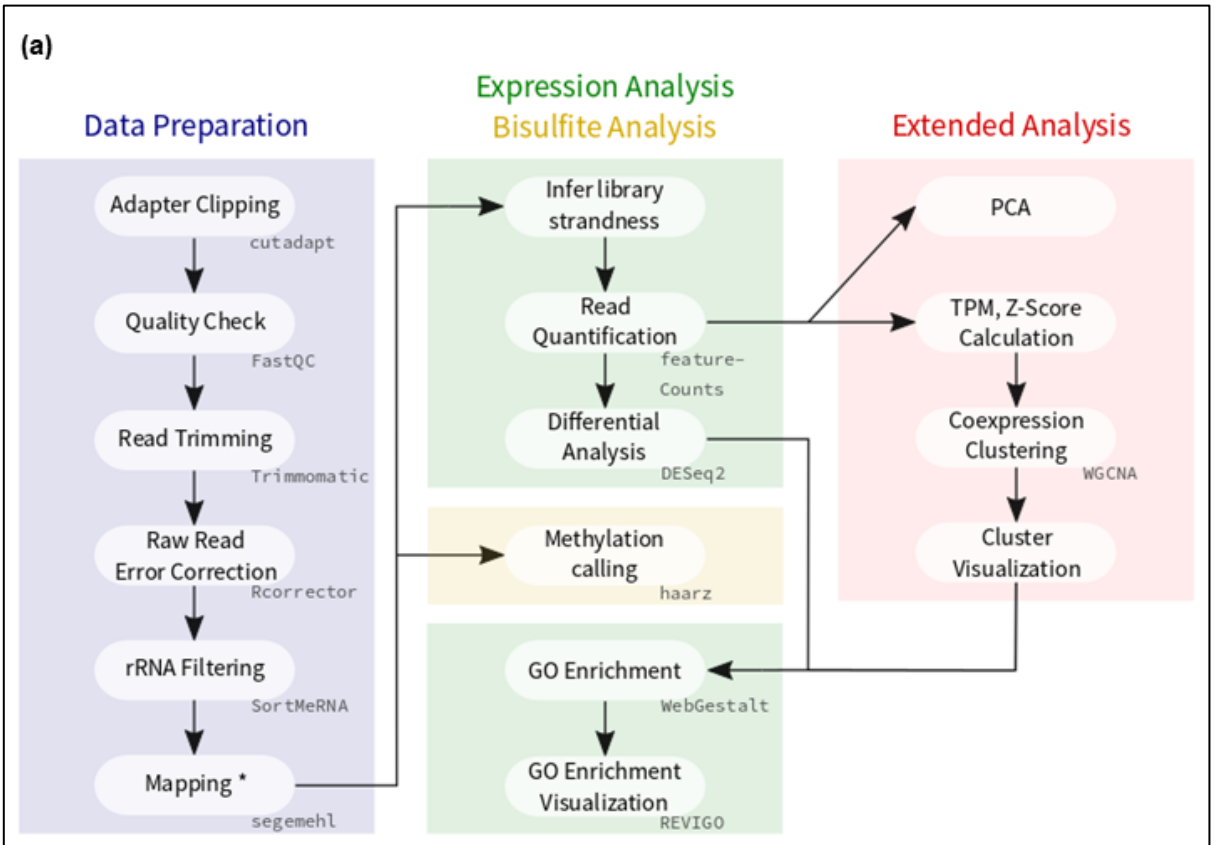


**Figure 5 : RNA-seq and WGBS analysis pipeline.**

**(a)** The schematic summarizes the pipeline used for analyzing the RNA-seq and WGBS data in this study. The names of the tools used at each respective steps are mentioned in the pipeline. (Schematic provided by Konstantin Riege)

# 8. Results

## 8.1. FACS of B-cells in different stages of tumorigenesis

The Eμ-Myc mice have a c-Myc transgene expressed under the control of IgH enhancer which leads to c-Myc overexpression specifically in the B-cell lineage. This overexpression leads to the development of spontaneous B-cell lymphomas in Eμ-Myc mice. Tumor B-cells enrich in lymph nodes around the age of 10-12 weeks. In order to isolate the intermediate stages of tumorigenesis, pre-tumor B-cells were obtained from the spleen of Eμ-Myc mice at 8-10 weeks of age, with no visible tumor development.

To isolate unique cell populations, wild-type and pre-tumor B-cells were purified via FACS. CD19 is a bonafide B-cell surface marker while surface levels of B220 (Protein tyrosine phosphatase receptor type, C) are known to reduce with lymphomagenesis (Croxford et al., 2013). All the wild-type B-cells have high B220 levels (Fig 6a). On the other hand, pre-tumor mice had two distinct B-cell populations with high and low surface levels of B220 (Fig 6a). The pre-tumor high cells are benign (wild-type like) while pre-tumor low cells are at an early stage of transformation (tumor-like). The tumor B-cells being enriched in lymph nodes did not require sorting. The tumor B-cells were stained post-isolation for CD19, B220 and IgM markers and isolations with purity of ~95% for CD19+/ B220 low/ IgM− tumor B-cells were selected for downstream analysis (Fig 6a).

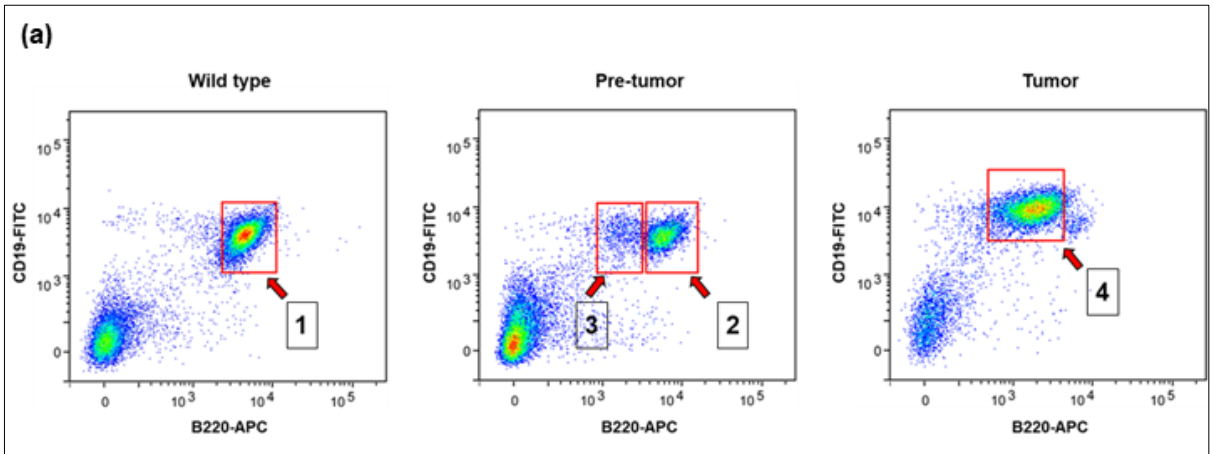


**Figure 6 : FACS plots for cells in different stages of tumorigenesis.**

**(a)** The plots show levels of cell surface markers B220 on X-axis (B220-APC) and CD19 on Y-axis (CD19-FITC). The red boxes in each FACS plot mark the populations of B-cells isolated in this study: wild-type (1), pre-tumor high (2), pre-tumor low (3) and tumor cells (4).

## 8.2. Ribosomal DNA transcription regulation during tumorigenesis

### 8.2.1. Pre-rRNA levels increase during tumorigenesis

Transcriptional upregulation of pre-rRNA, enlarged nucleoli and increased ribosome biogenesis are characteristic features of most cancer cells (Pelletier et al., 2018). However, it remains unclear if higher pre-rRNA transcription is required for the sustenance of pre-malignant cells and if so how the epigenetic regulation at the rDNA locus is altered during tumorigenesis.

We first quantified the levels of pre-rRNA at different stages of tumorigenesis and compared them to the pre-rRNA levels in wild-type cells. The pre-rRNA primers used in RT-PCR amplify the region flanking the first processing site in pre-rRNA at 5' end (Mullineux and Lafontaine, 2012). The levels of pre-rRNA were normalized to beta-2 microglobulin (B2M) mRNA levels.

The pre-tumor high and pre-tumor low cells show a significant increase of ~2.3 fold and ~2.1 fold compared to wild-type cells respectively (Fig 7a). The pre-rRNA levels were highest for tumor cells, ~11 fold higher compared to wild-type cells (Fig 7a). Variation in the extent of increase in the pre-rRNA levels was observed in tumor cells from different Eμ-Myc mice. This we think is an outcome of different levels of Myc overexpression, a positive regulator of rDNA transcription and processing, in each individual Eμ-Myc mice (Arabi et al., 2005; Lefebure et al., 2017; Schlosser et al., 2003). The increased pre-rRNA levels in the pre-tumor high and low cells could be an outcome of Myc overexpression in both these cells compared to wild-type cells. On the other hand, we think that the drastic increase in pre-rRNA levels in the tumor cells compared to pre-tumor cells is coupled more with tumor transformation than with Myc overexpression. Therefore, we conclude that tumorigenesis in the Eμ-Myc mice is associated with increasing levels of pre-rRNA.

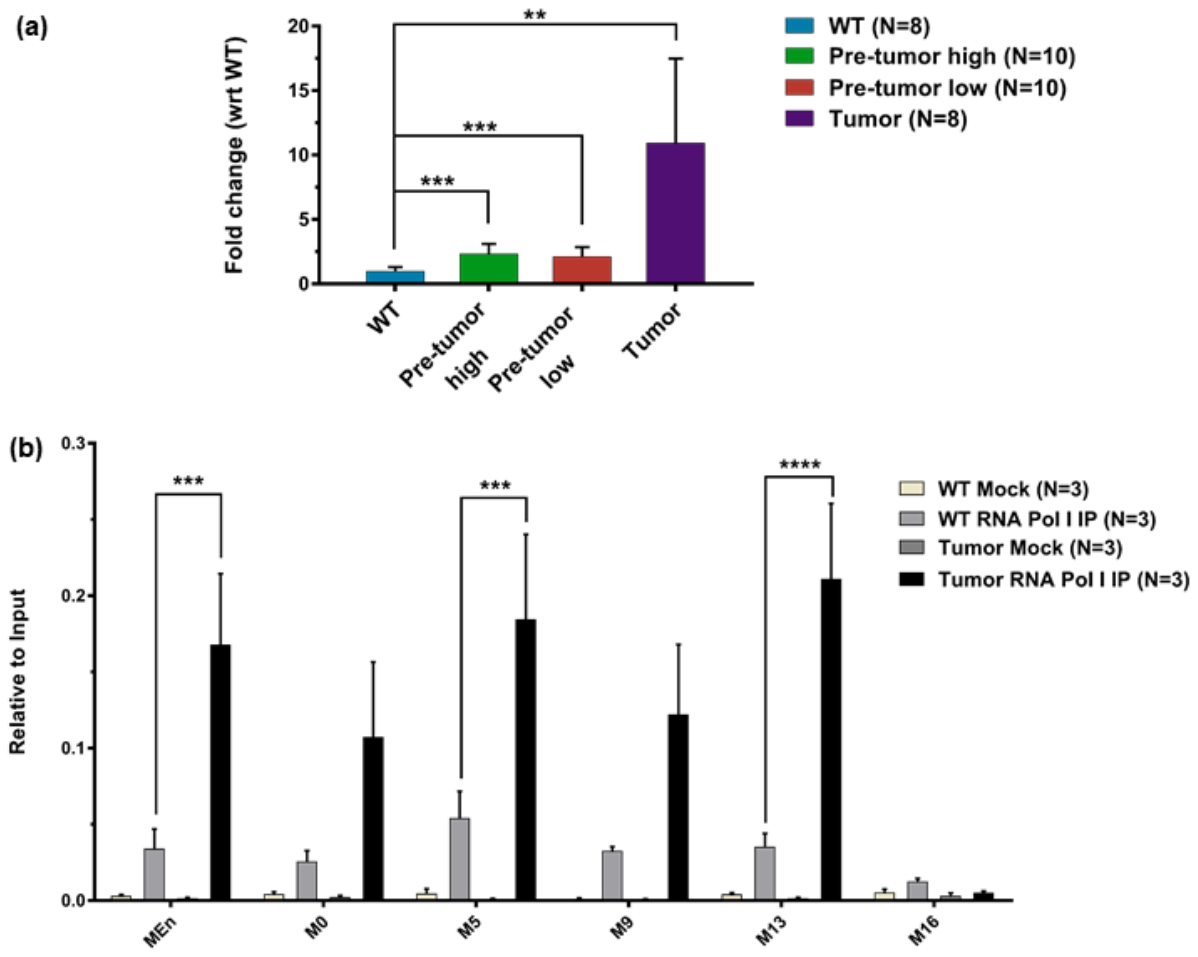


**Figure 7 : Ribosomal DNA transcription increases during tumorigenesis.**

**(a)** Quantification of pre-rRNA expression in WT, pre-tumor high, pre-tumor low and tumor cells obtained from qRT-PCR. Normalization was performed using B2M RNA levels. Student t-test used for statistical analysis (**:p<0.01, ***:p<0.001).

**(b)** Quantification of RNA Polymerase I occupancy on rDNA using primers amplifying enhancer region (MEn), promoter region (M0), gene body region (M5, M9, M13) and region beyond transcription termination site (M16) using qPCR. Normalization performed with respect to input chromatin. Two way Anova test used for statistical analysis (***:p<0.001, ****:p<0.0001).

### 8.2.2. RNA Pol I occupancy on rDNA increases in tumor cells

Albeit pre-rRNA levels have been shown to well reflect Pol I transcriptional activity, elevated levels can also be caused by reduced pre-rRNA processing. To rule out the latter possibility, we performed ChIP for RNA Pol I occupancy at the rDNA in wild-type and tumor cells. Chromatin co-precipitated with an antibody raised against RPA116, the second largest Pol I subunit, was analyzed in qPCR with primers

amplifying regions in enhancers (MEn), promoter (M0), gene body (M5, M9, M13) and intergenic spacer region (M16, downstream of transcription termination site) of the rDNA gene (primer sequences adapted from O'Sullivan et al., 2002). Compared to wild-type cells, the tumor cells showed a significant increase in RNA Pol I occupancy in all regions tested except the M16 site, where as expected, virtually no Pol I binding could be detected (Fig 7b). Specificity of the ChIP was demonstrated by the lack of rDNA precipitation when the anti-RPA116 antibody was omitted in the mock controls (Fig 7b). Therefore, we conclude that the increased levels of pre-rRNA in tumor cells is due to augmented transcription.

### 8.2.3. Fraction of promoter-methylated rDNA repeats increase during tumorigeneis

In mice, transcription is inhibited from the rDNA repeats having a methylated promoter, with cytosine -133 being the crucial methyl-acceptor site (Santoro and Grummt, 2001). A decrease in this promoter methylation could reactivate the rDNA repeats and therefore explain the increased pre-rRNA transcription during tumorigenesis. To test this hypothesis, the fraction of promoter-methylated rDNA repeats was quantified using CHOP-qPCR assay.

Surprisingly, there was a significant increase of ~1.5 fold in the fraction of promoter-methylated rDNA repeats for both pre-tumor high and pre-tumor low cells in comparison with wild-type cells (Fig 8a). The fraction of promoter-methylated rDNA repeats increased slightly further in tumor cells to ~1.7 fold in comparison with wild-type cells (Fig 8a). Given this counterintuitive correlation between enhanced Pol I activity and increased promoter methylation, we wondered whether rDNA in the pre-malignant and tumor states acquires 5-hydroxymethylated cytosine (5-hmC). 5hmC is known to be permissive for transcription (Greco et al., 2016), but cannot be distinguished from cytosine methylation by the CHOP-qPCR assay. Therefore, we quantified the 5-hmC levels in rDNA promoter using the glucosyltransferase enzyme based method. However, 5-hmC levels were in general very low at the rDNA promoter and did not change during tumorigenesis (Fig 8b), suggesting that silencing of more rDNA repeats occurs simultaneously with an overall transcriptional upregulation from rDNA.

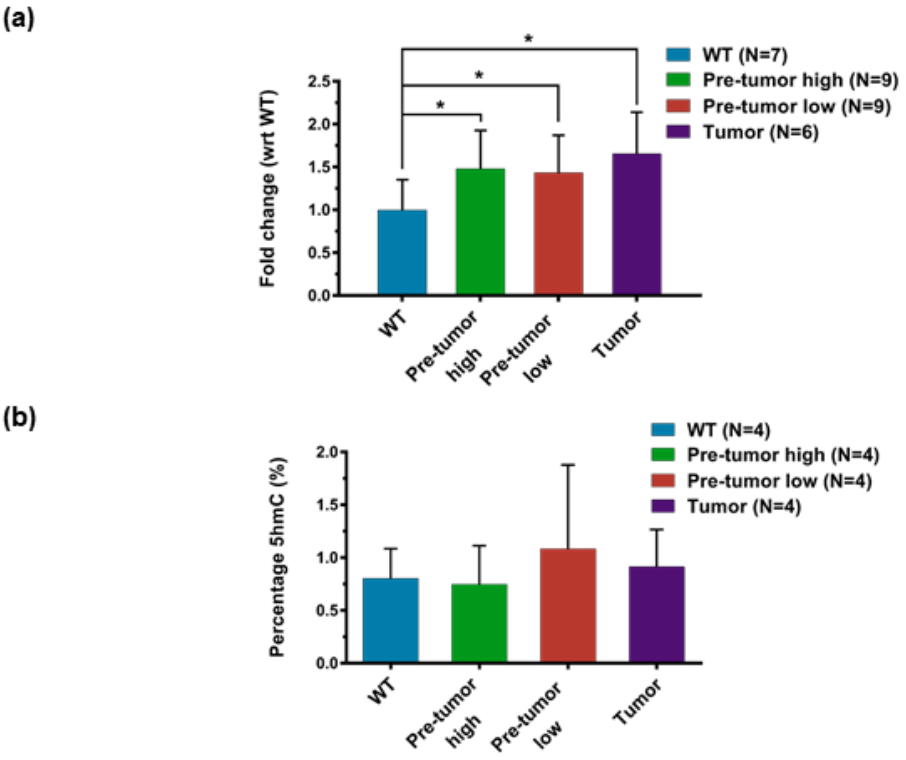


**Figure 8 : Fraction of promoter-methylated ribosomal DNA repeats increases during tumorigenesis.**

**(a)** Quantification for rDNA promoter methylation in WT, pre-tumor high, pre-tumor low and tumor cells obtained from CHOP-qPCR. Student t-test used for statistical analysis (*:p<0.05).

**(b)** Quantification for rDNA promoter 5-hmC levels in WT, pre-tumor high, pre-tumor low and tumor cells. No statistically significant difference in 5-hmC levels observed on performing student t-test.

### 8.2.4. Promoter RNA expression increases with tumorigenesis

The rDNA promoter methylation is under the control of nucleolar remodeling complex (NoRC) which acts as a platform for recruiting chromatin-modifying enzymes which silence the rDNA repeats (Strohner et al., 2001; Santoro et al. 2005). The NoRC complex is targeted to the rDNA promoter by a non-coding RNA transcribed by RNA Pol I from the intergenic spacer in sense orientation, called promoter RNA (pRNA) (reviewed in Bierhoff et al., 2010). Increased levels of pRNA, therefore, would lead to increased recruitment of NoRC complex to rDNA promoter and explain the relative increase in the methylated rDNA fraction shown in Figure 8a. Hence, we quantified the levels of pRNA in RT-PCR using the mrDNA -205/-185→mrDNA -21/-1 primer pair. The pRNA levels were normalized to the levels of B2M.

There was no significant increase in pRNA levels in pre-tumor high cells compared to wild-type cells (Fig 9a). While the pre-tumor low and tumor cells showed a significant increase of ~3 fold and ~12 fold compared to wild-type cells respectively (Fig 9a). The increase in pRNA levels in pre-tumor low and tumor cells in comparison with wild-type cells could therefore explain corresponding increased fraction of promoter-methylated rDNA repeats. However, the pRNA levels do not change in the pre-tumor high cells where we did observe an increased fraction of promoter-methylated rDNA repeats (Fig 8a). Hence, possibly an alternate mechanism for DNA methylation in the rDNA promoter could be involved. That being said, the increased levels of pRNA specifically for the pre-tumor low (tumor-like) and tumor cells hints at a role of pRNA in silencing and stabilizing rDNA repeats during tumorigenesis.

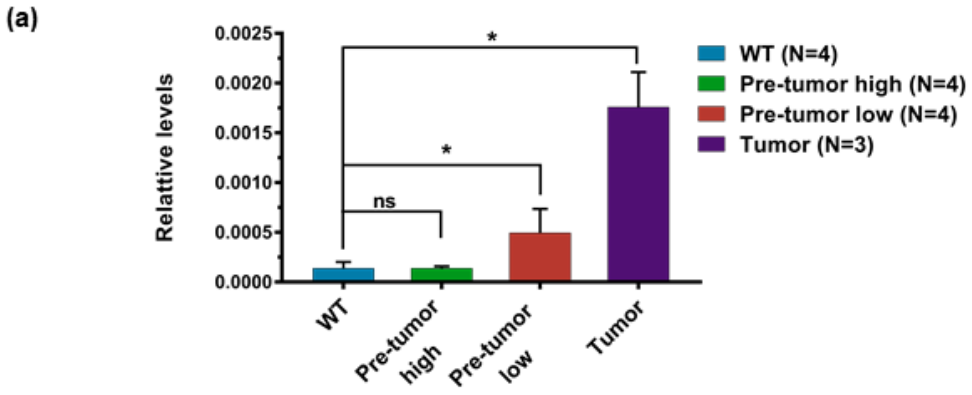


**Figure 9 : pRNA levels increase with tumorigenesis.**

**(a)** Quantification of pRNA expression in WT, pre-tumor high, pre-tumor low and tumor cells obtained from qRT-PCR. Normalization was performed using B2M RNA levels. Student t-test used for statistical analysis (*:$p<0.05$).

### 8.2.5. rDNA copy number loss occurs in tumor cells

The high rates of rDNA transcription observed in pre-tumor and tumor cells possibly increase the instability at the rDNA locus. The resulting loss of active rDNA repeats would be another explanation for the relative increase in the methylated rDNA fraction shown in Figure 8a. However, the pre-tumor high and pre-tumor low cells did not show significant changes in the rDNA copy numbers compared to wild-type cells (Fig 10a). On the contrary, tumor cells showed a significant reduction in the rDNA copy numbers by ~20% (Fig 10a). This loss of rDNA repeats does not explain the ~50% increase in promoter-methylated rDNA repeats during tumorigenesis observed in

Figure 8a. Therefore, we conclude that the increased fraction of promoter-methylated rDNA repeats observed in Figure 8a is not an outcome of loss of active rDNA repeats but indeed a result of *de novo* methylation at rDNA promoter.

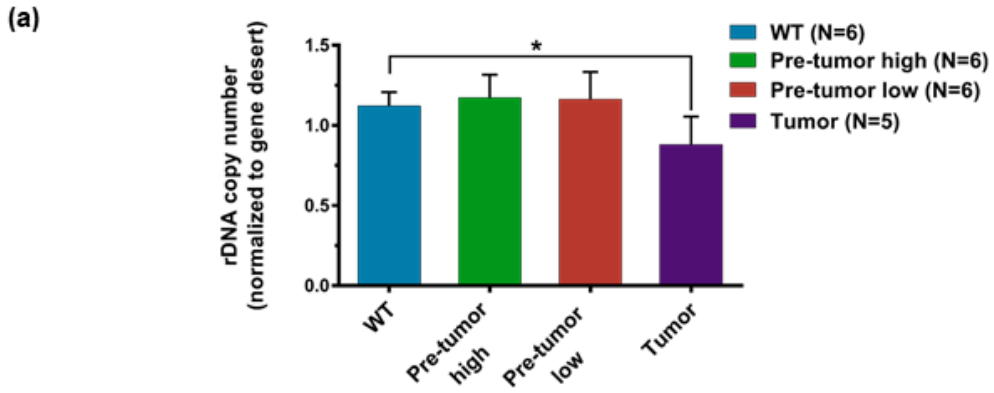


**Figure 10 : Ribosomal DNA copy number loss occurs in tumor cells.**

**(a)** Quantification of rDNA copy number in WT, pre-tumor high, pre-tumor low and tumor cells obtained from qPCR. Input DNA normalization was done using single copy gene desert region on Chr 15. Student t-test used for statistical analysis (*:p<0.05).

### 8.2.6. Myc overexpression is sufficient to increase the fraction of promoter-methylated rDNA repeats

The fraction of promoter-methylated rDNA repeats was increasing in the cells yet to become tumorigenic i.e. pre-tumor high and pre-tumor low cells of Eμ-Myc mice while the rDNA copy number loss was observed only in tumor cells. Therefore, we hypothesize that overexpression of Myc in the pre-tumor cells of Eμ-Myc mice in comparison to wild-type cells is causing an increase in the fraction of promoter-methylated rDNA repeats. On the other hand, loss of rDNA repeats is an outcome of massive pre-rRNA transcription essential for tumor cell survival.

To test this hypothesis, we overexpressed Myc in NIH3T3 mouse fibroblasts and analyzed the status of rDNA transcription, fraction of promoter-methylated rDNA repeats and rDNA copy numbers. An about 6-fold Myc overexpression of Myc was confirmed through western blotting (Fig 11a), which led to ~3 fold increase in pre-rRNA levels (Fig 11b), consistent with Myc being a positive regulator of rDNA transcription (Arabi et al., 2005). Importantly, overexpression of Myc resembled the epigenetic and the copy number changes of B-cell lymphomas, i.e. promoter-methylated rDNA repeats increased while rDNA copy number decreased by ~40% compared to control

NIH3T3 cells (Fig 11c and 11d). Therefore, we conclude that Myc overexpression possibly leads to *de novo* promoter methylation of rDNA repeats and increased transcription induces instability resulting in rDNA copy number losses.

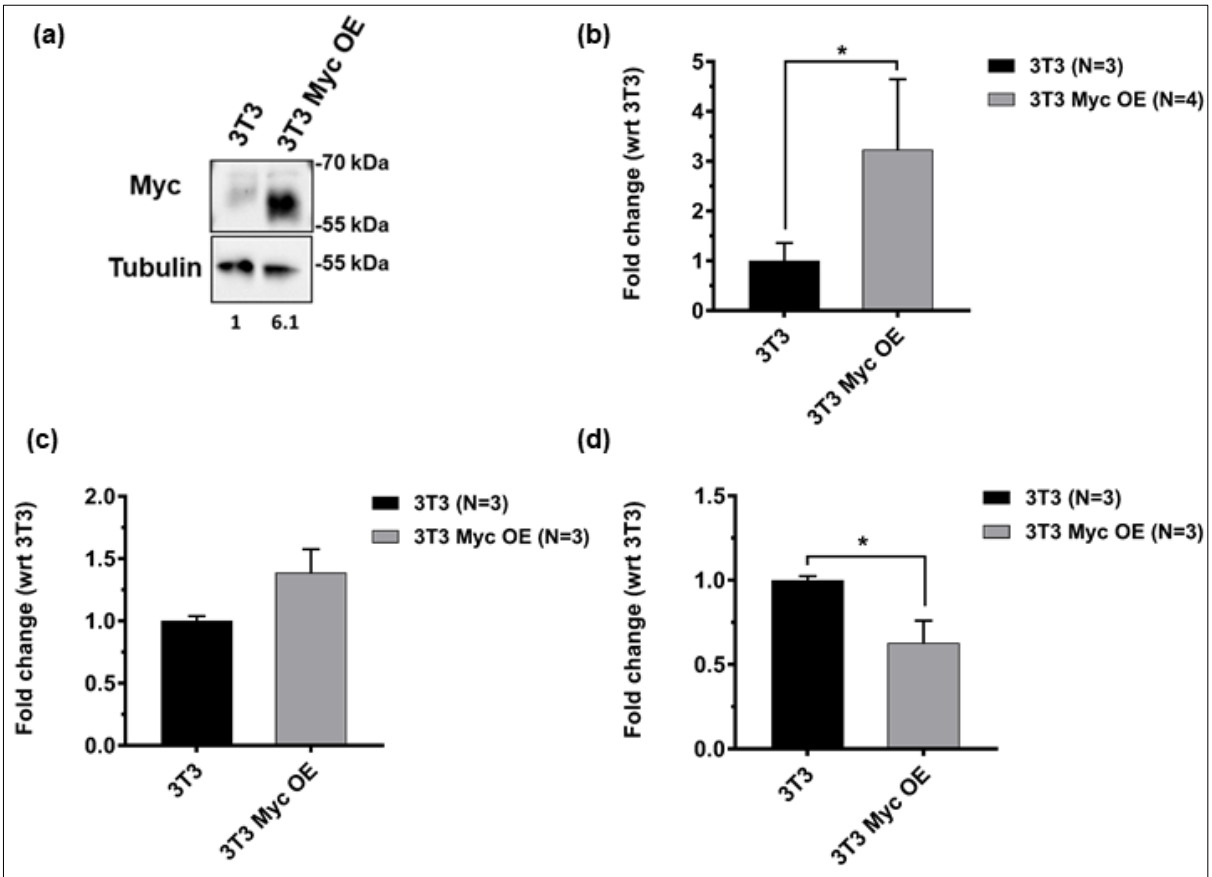


**Figure 11 : Increase in fraction of promoter-methylated ribosomal DNA repeats upon Myc overexpression.**

**(a)** Western blot showing protein levels of Myc in wild type and Myc overexpressing 3T3 cells. Tubulin was used as loading control.

**(b)** Quantification of pre-rRNA expression in 3T3 WT and Myc overexpressing 3T3 Myc OE cells obtained from qRT-PCR. Normalization was performed using B2M RNA levels. Student t-test used for statistical analysis (*:$p<0.05$).

**(c)** Quantification of rDNA promoter methylation in 3T3 WT and 3T3 Myc OE cells obtained from CHOP-qPCR. Student t-test showed no significant increase possibly due to limited number of replicates.

**(d)** Quantification of rDNA copy number in 3T3 WT and 3T3 Myc OE cells obtained from qPCR. Input DNA normalization was done using single copy gene desert region on Chr 15. Student t-test used for statistical analysis (*:$p<0.05$).

## 8.3. Regulation of transcriptome and DNA methylome during tumorigenesis

### 8.3.1. RNA-seq reveals unique transcriptome for each stage of tumorigenesis

The RNA-seq analysis presented here is based on two biological replicates for wild-type, pre-tumor low and tumor cells except for pre-tumor high cells which are in four replicates. While more replicates of each state have been generated and are currently in the sequencing phase, preliminary bioinformatic analysis of the available samples has been conducted. The number of differentially expressed genes with respect to wild-type cells increased significantly as cells moved towards tumor state. The pre-tumor high cells (wild-type like) showed ~600 deregulated genes, pre-tumor cells (tumor-like) showed ~3000 deregulated genes while tumor cells showed ~6000 deregulated genes, with minimum two-fold change.

Principal component analysis compared the whole transcriptomes of each stage of tumorigenesis (Fig 12a). The biological replicates for wild-type, pre-tumor high, pre-tumor low and tumor cells clustered together establishing consistency of gene expression across biological replicates. In the PCA plot, the transcriptome of pre-tumor high cells was closest to wild-type cells while the transcriptome of pre-tumor low cells was approximately equally distant from wild-type and tumor cells. Thus, one can qualitatively observe the tumor progression through this PCA plot (Fig 12a).

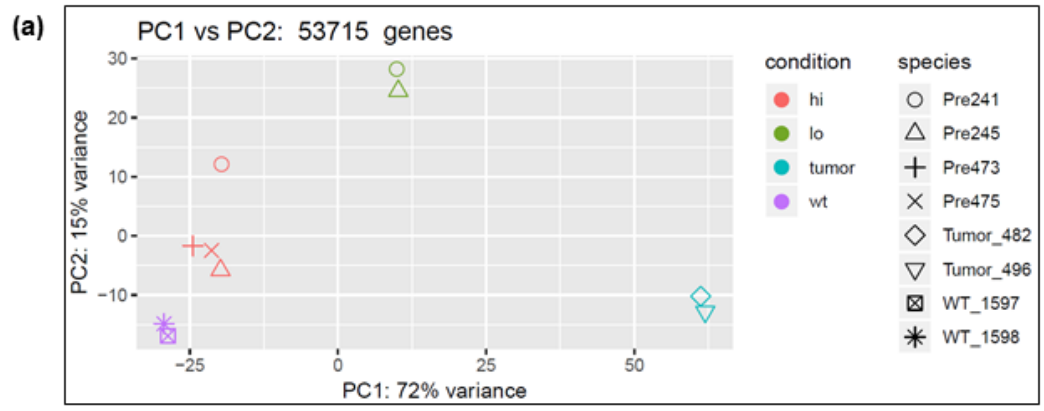


**Figure 12 : Principal component analysis of RNA-seq data.**

**(a)** Principal component analysis plot of RNA-seq data for all biological replicates of WT (N=2), pre-tumor high (N=4), pre-tumor low (N=2) and tumor cells (N=2). PCA analysis and the figure provided by Konstantin Riege.

### 8.3.2. Expression trends of epigenetic regulators during tumorigenesis

We were interested in analyzing the mechanism for changes in DNA methylation in the context of bivalent chromatin regions during tumorigenesis. Therefore, as a crude preliminary analysis, we identified gene expression trends for regulators of DNA methylation and histone modifications from our RNA-seq data. The gene expression changes for epigenetic modifiers such as DNMTs, TET, histone methyltransferases (HMTs), histone demethylases (HDMs), histone acetyltransferases (HATs) and histone deacetylases (HDACs) were extracted. Out of all those epigenetic modifiers, the ones with more than two-fold significant change in expression in at least one stage of tumorigenesis are represented in the form of a heatmap (Fig 13a).

Interestingly, DNMT1 and DNMT3b showed a gradual increase in expression with tumorigenesis. Transcription of MLL family of histone methyltransferases, responsible for H3K4 methylation reduced significantly with tumorigenesis. On the other hand, transcription of EZH2, the enzymatic component of polycomb repressive complex (PRC2) involved in H3K27 methylation increased significantly with tumorigenesis. These two changes if translated to protein levels could explain the loss of bivalency during tumorigenesis. The other striking class of deregulated enzymes were the HDMs, which significantly decrease with tumorigenesis. On the other hand, HATs, HDACs and SWI/SNF chromatin remodeling proteins do not follow a common trend in expression during tumorigenesis. Therefore, we see characteristic changes in gene expression patterns of epigenetic modifiers involved in regulation of DNA methylation and bivalent histone modifications during tumorigenesis.

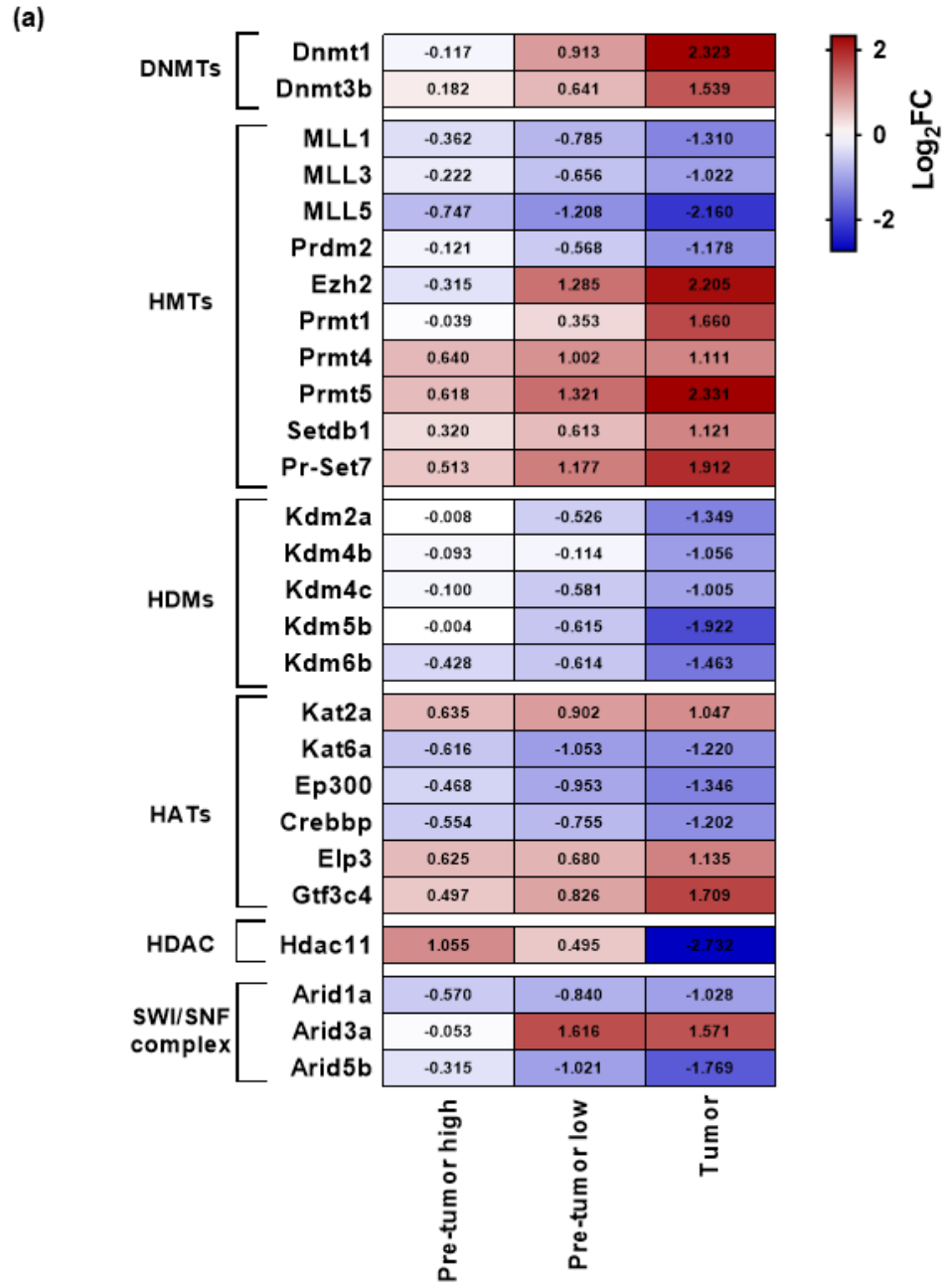


**Figure 13 : Expression trends of epigenetic regulators during tumorigenesis.**

**(a)** Heatmaps represent the changes in expression of epigenetic regulators such as DNMTs, HMTs, HDMs, HATs, HDACs and components of the SWI/SNF chromatin remodelling complex. The $log_2$fold-change values with respect to wild-type cells are represented in each individual box.

### 8.3.3. Developmental genes are transiently upregulated in pre-tumor low cells

FBS were shown to be hypermethylated in cancer cells but also show increased transcription of the associated developmental genes (Bernhart et al., 2016). Untimely expression of developmental genes could provide wild-type cells with a window of transformation and hence understanding the basis of their transcription regulation is critical. However, the Bernhart et al. study was limited due to a lack of information on the temporal order of epigenetic changes during tumorigenesis. The tumors are also usually a heterogeneous mass of cells in pre-tumor and tumor stages providing us with an averaged view of expression and epigenetic changes. In our study, we have overcome these limitations and have analysed the expression of FBS associated developmental genes in the tumorigenesis model.

The genomic locations of FBS are not mapped in the mouse genome. Hence, we lifted over the FBS identified in the human genome into the mouse genome based on sequence similarity using the UCSC liftover tool (Bernhart et al., 2016; Haeussler et al., 2019). This preliminary liftover though crude is highly likely to match the actual FBS locations for mouse, given a recent study showing conserved DNA motifs for respective histone modifications in human and mouse (Ngo et al., 2019). With the liftover tool, ~900 FBS identified in the human genome mapped to ~800 locations in the mouse genome.

The change in expression levels from the genes associated with these FBS was analyzed. Pre-tumor high cells showed 11 genes, pre-tumor low cells showed 66 genes while tumor cells showed 79 genes with significant deregulation (FBS-GE) in comparison with wild-type cells (Fig 14a). The rest of the significantly deregulated non-FBS genes in the respective stages during tumorigenesis were taken as background control genes (BG-GE).

The median value of $\log_2$-fold expression change in the FBS associated genes was calculated for each stage during tumorigenesis (FBS-GE) compared to wild-type cells. Interestingly, the median $\log_2$-fold expression change for these genes in pre-tumor low cells was significantly higher (~2.5 fold) than pre-tumor high and tumor cells (Fig 14a). Thus, we observe a pulse of increased expression for genes associated with FBS during tumorigenesis, specifically in pre-tumor low cells. The background genes, on the other hand, show no significant change in the median $\log_2$-fold expression change between different stages of tumorigenesis (BG-GE). The median

of $log_2$-fold expression change in all the stages of tumorigenesis was greater than one possibly due to Myc being a general transcription activator.

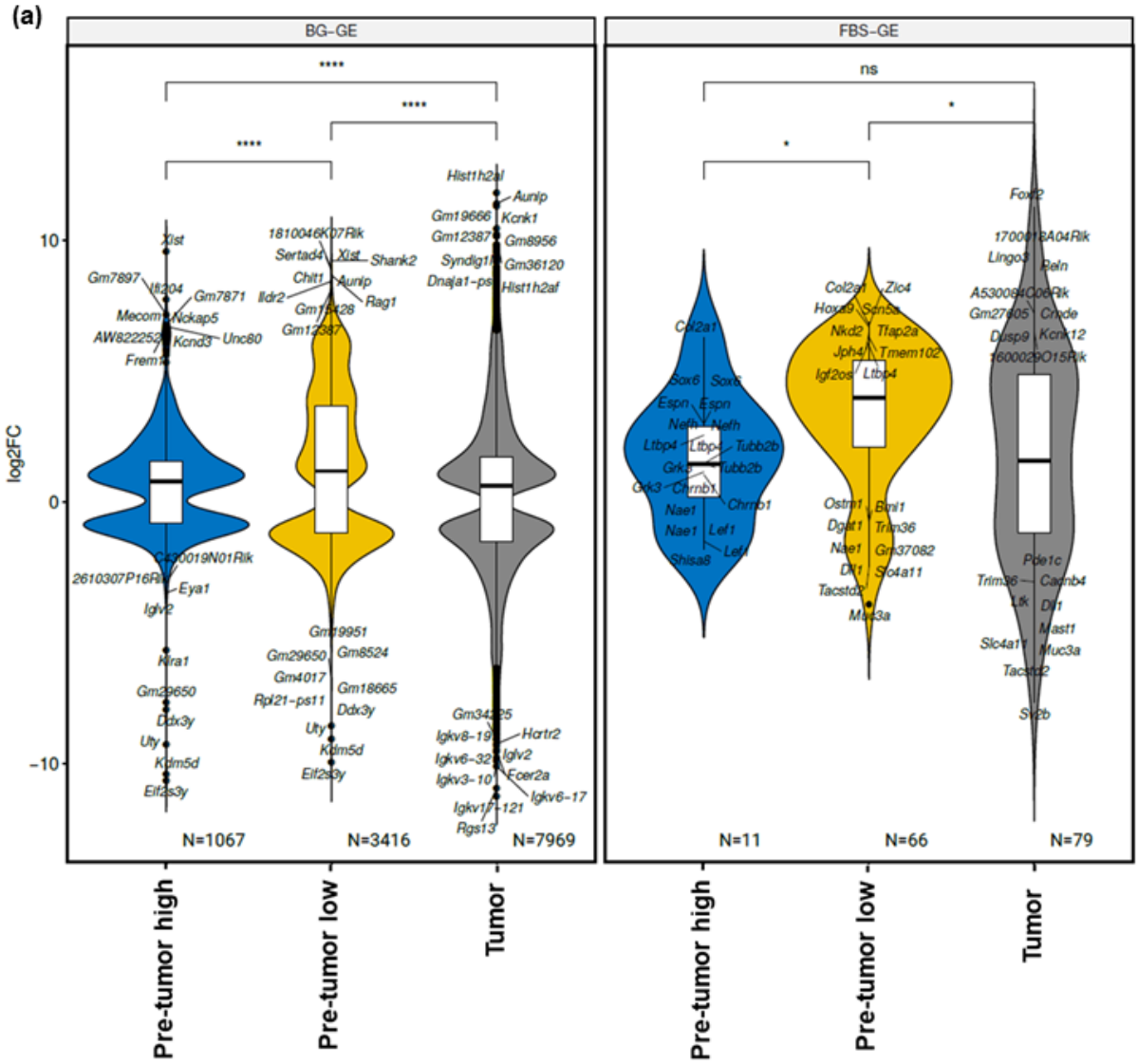


**Figure 14 : Developmental genes show transient increase in expression during tumorigenesis.**

(a) The distribution of $log_2$-fold changes wrt WT cells in background (left box, BG-GE) and FBS associated developmental genes (FBS-GE) are represented in the form of violin plots for each stage of tumorigenesis. Each violin plot shows the median of $log_2$-fold expression change for significantly deregulated genes at that stage of tumorigenesis. The distributions are compared using unpaired Krusall-Wallis non-parametric test (*:p<0.05, ****:p<0.0001). Figure provided by Konstantin Riege.

### 8.3.4. Developmental gene expression increases despite an increase in DNA methylation

The preliminary analysis of the WGBS was limited to the FBS, as the genes associated with these FBS showed a significant transient increase in expression in the pre-tumor cells (Fig 14a). We will eventually process the differential methylation rates on the genome-wide level and analyze changes in other functional chromatin segments such as promoter, enhancer, etc.

The change in expression of the FBS associated developmental genes is expressed in terms of $log_2$-fold change ($log_2FC$) while the DNA methylation change in the FBS is expressed as the difference in DNA methylation rate (Delta me) (Fig 15). We were interested in genes showing positive dependence between DNA methylation and gene expression (genes belonging to the first and third quadrant of the scatter plots). The pre-tumor high cells show deregulation of only 11 FBS associated genes out of which 8 genes are with positive dependence (Fig 15a). In the pre-tumor low cells, there is a significant increase in the number of deregulated FBS associated genes to 67 out of which 42 show positive dependence (Fig 15b). In the tumor cells, there are 79 deregulated FBS associated genes out of which 44 genes show positive dependence (Fig 15c).

Thus, we observe a significant number of developmental genes associated with FBS to have increased gene expression despite of increased DNA methylation in the FBS. However, one needs to interpret the currently presented results cautiously as the change in DNA methylation in the FBS is an averaged value calculated for change in methylation of all cytosines present in that FBS. Therefore, our upcoming analysis from this WGBS data would look for nucleotide level methylation changes in the promoter of these developmental genes.

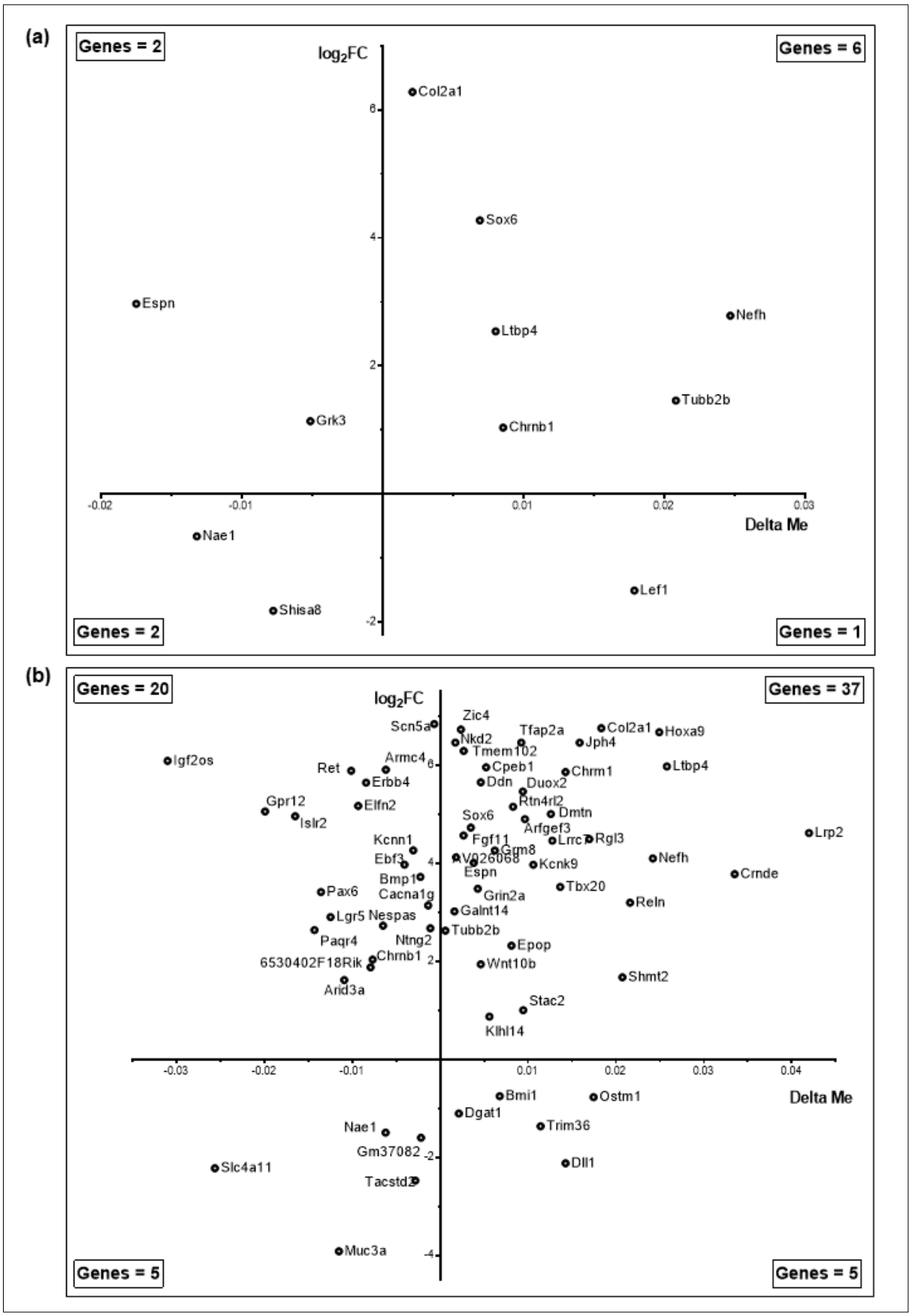
(a)
Genes = 2
log2FC
Genes = 6
Col2a1
Sox6
Espn
Nefh
Ltbp4
Tubb2b
Grk3
Chrnb1
Nae1
Lef1
Shisa8
Genes = 2
Genes = 1
Delta Me
(b)
Genes = 20
log2FC
Genes = 37
Zic4
Scn5a
Tfap2a
Col2a1
Hoxa9
Nkd2
Jph4
Tmem102
Igf2os
Armc4
Cpeb1
Chrm1
Ltbp4
Ret
Erbb4
Ddn
Duox2
Rtn4rl2
Gpr12
Elfn2
Dmtn
Islr2
Sox6
Arfgef3
Lrp2
Kcnn1
Fgf11
Lrrc7
Rgl3
Ebf3
Gm8
Nefh
Kcnk9
Espn
Crnde
Bmp1
Tbx20
Pax6
Cacna1g
Grin2a
Reln
Galnt14
Lgr5
Nespas
Tubb2b
Paqr4
Ntng2
Epop
6530402F18Rik
Chrnb1
Wnt10b
Shmt2
Arid3a
Stac2
Klhl14
Bmi1
Ostm1
Delta Me
Dgat1
Nae1
Trim36
Gm37082
Slc4a11
Dll1
Tacstd2
Muc3a
Genes = 5
Genes = 5

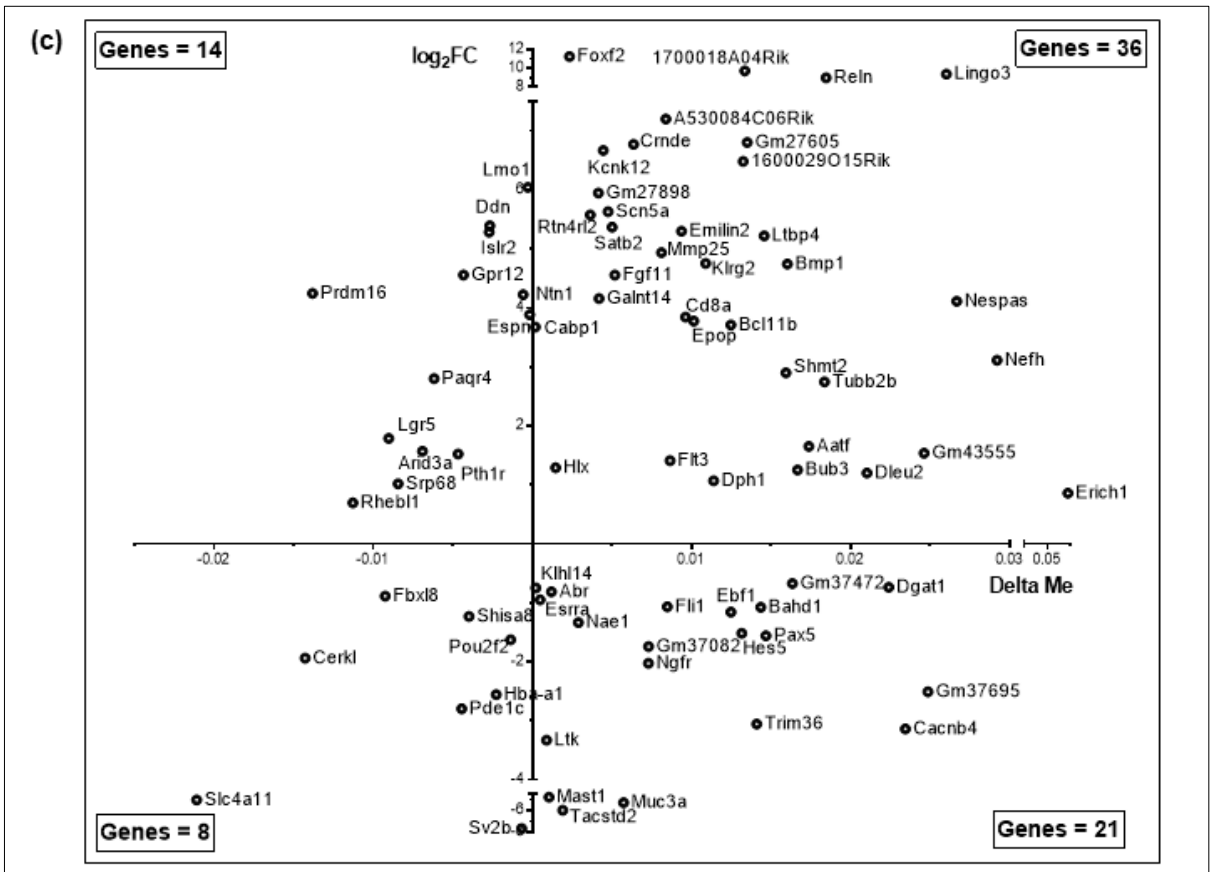


**Figure 15 : DNA methylation and gene expression changes during tumorigenesis.**

The scatter plots show change in rate of DNA methylation in the FBS (Delta me, X-axis) vs $log_2$-fold change in gene expression of the associated developmental gene ($log_2$-fold change (log2FC, Y-axis) for pre-tumor high (a), pre-tumor low (b) and tumor cells (c) compared with wild-type cells. The number of genes in each quadrant are mentioned for each scatter plot.

# 9. Discussion and future perspectives

Epigenetic regulators play a significant role in the regulation of pre-rRNA transcription which is the key step in ribosome biogenesis. Cancer cells show high proliferation rates and therefore need higher levels of ribosomes to meet with their protein synthesis requirements (Derenzini et al. 2017). In our study, we analyzed the changes in epigenetic regulation of rDNA transcription during tumorigenesis.

We observed a significant increase in pre-rRNA synthesis in the tumor cells with a counterintuitive increased fraction of promoter-methylated rDNA repeats (Fig 7a and 8a). We propose a role of NoRC complex, based on the increased pRNA transcription and gene expression of the epigenetic modifiers associated with NoRC complex (DNMT1, DNMT3b and Setdb1), in *de novo* methylation of rDNA repeats during tumorigenesis (Schmitz et al. 2010; Santoro et al. 2005) (Fig 9a and 13a). The increased RNA Pol I binding in the rDNA enhancer region, located immediately downstream of pRNA promoter, further supports the increased pRNA transcription (Fig 7b). However, we do not see an increase in pRNA levels in the pre-tumor high cells, which do have increased promoter-methylated rDNA repeats. Therefore, we need to quantify the occupancy of pRNA and NoRC complex at the rDNA promoter to confirm the role of pRNA in mediating rDNA promoter methylation during tumorigenesis. We will be performing ChIP for TIP5, a component of NoRC complex which stabilizes pRNA at the rDNA promoter, for each stage of tumorigenesis.

Myc interacts with DNMT3b and recruits it to specific genomic locations to establish *de novo* DNA methylation (Poole et al. 2017). Also, we see an increase in promoter-methylated rDNA repeats just by overexpressing Myc in NIH3T3 cells (Fig 11c). Hence, another possible mechanism for the increase in promoter-methylated rDNA repeats would be via Myc-dependent recruitment of DNMT3b specifically at the Myc binding sites (E-box) present in the rDNA promoter (Arabi et al. 2005). Thus, we would perform ChIP for Myc and DNMT3b to quantify their occupancy both at the rDNA promoter, for each stage of tumorigenesis.

We hypothesize that increasing the fraction of promoter-methylated silent rDNA repeats is a tumor cell mechanism to safeguard its rDNA repeats from damages induced from cancer-associated high rates of rDNA transcription. On the other hand, to meet the high pre-rRNA synthesis requirements, tumor cells are likely to upregulate transcription from already active rDNA repeats, possibly via increased RNA Pol I

recycling and loading in the promoter (Fig 7b). This mechanism would not only provide the tumor cell with required higher pre-rRNA levels but would also safeguard its rDNA repeats which might be crucial for tumor cell ability to proliferate indefinitely.

We in fact do observe signs of transcription induced genomic instability leading to loss of rDNA repeats in the tumor cells (Fig 10a). One could further investigate for structural defects in the rDNA locus during tumorigenesis, by fluorescently tagging individual rDNA repeats using the molecular combing approach (Caburet et al. 2005).

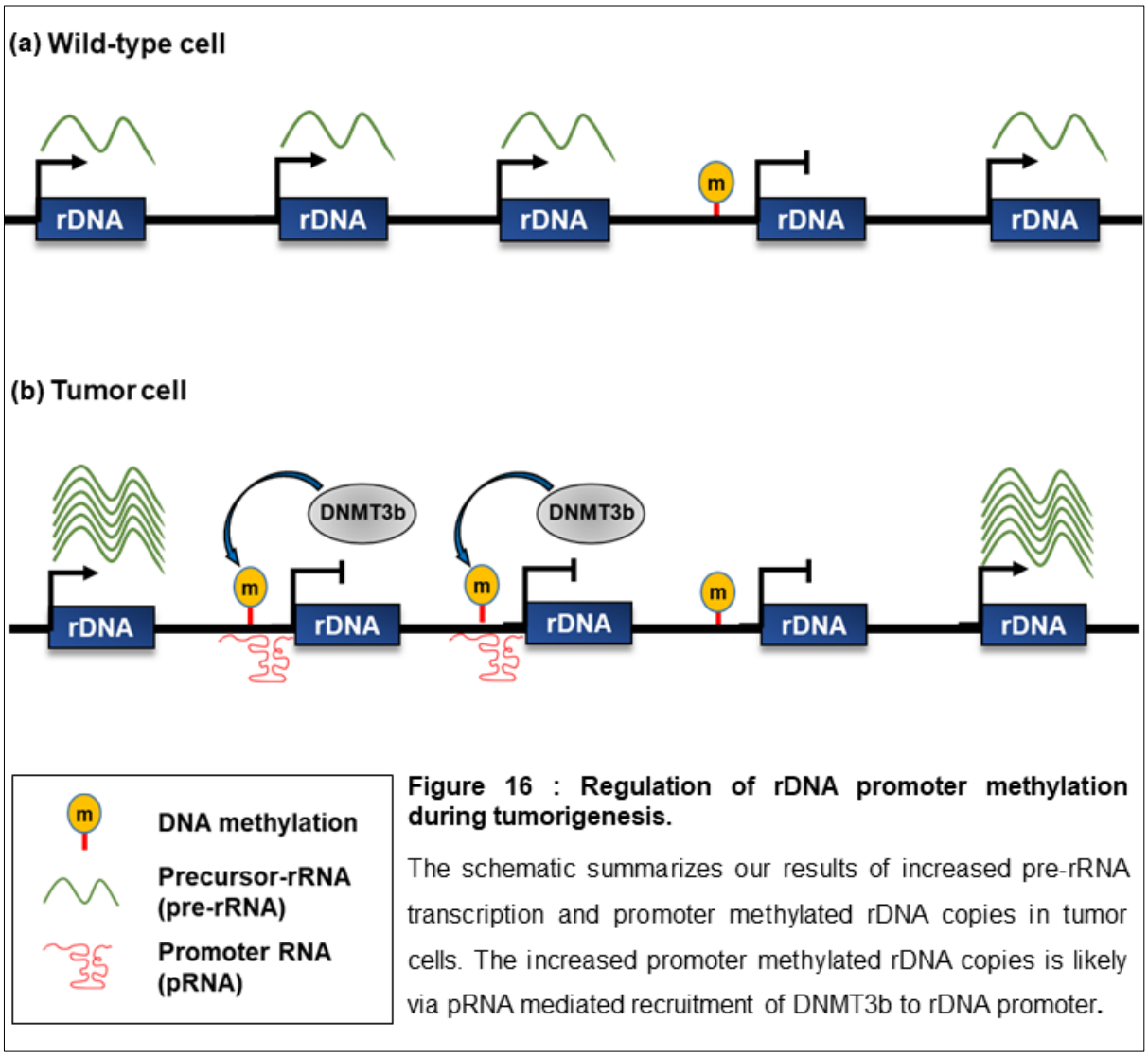


**Figure 16 : Regulation of rDNA promoter methylation during tumorigenesis.**

The schematic summarizes our results of increased pre-rRNA transcription and promoter methylated rDNA copies in tumor cells. The increased promoter methylated rDNA copies is likely via pRNA mediated recruitment of DNMT3b to rDNA promoter.

The results from RNA-seq and WGBS presented in our study investigating the interplay between DNA methylation and gene expression from bivalent regions though preliminary, provide interesting directions for future experiments. The FBS associated developmental genes show a transient increase in expression in the pre-tumor low cells (Fig 14a). A significant proportion of these FBS associated developmental genes with increased expression also show increased DNA methylation as early as in the

pre-tumor low cells (Fig 15). The increased DNA methylation at the bivalent regions could be an outcome of instability of bivalent regions in tumor cells (Bernhart et al., 2016). Our RNA-seq data gives us some novel insight into the temporal order of deregulation in bivalency and DNA methylation during tumorigenesis (Fig 13a). The gene expression of DNMT1 and DNMT3b increase gradually during tumorigenesis. Interestingly, a simultaneous reduced gene expression of MLL family, histone writers responsible for H3K4 methylation and increased expression of EZH2, a histone writer of H3K27 methylation is observed early from the pre-tumor low cells. A loss of activatory H3K4 methylation from the bivalent regions due to decreased levels of MLL proteins would make the bivalent chromatin sites prone for DNA methylation by DNMTs leading to hypermethylation of bivalent regions (Fig 15). Hence, we could perform mass spectroscopy experiments to quantify changes in the proteome during tumorigenesis to draw any further conclusions. Also currently we have mapped the FBS in mouse by liftover from human FBS, which is not the most efficient method. Therefore, in the next stage of this study we would map the genome-wide occupancy of bivalent histone marks for each stage of tumorigenesis. For this we would implement the CUT&RUN approach of chromatin profiling to overcome the limitation posed from low cell numbers in the pre-tumor state (Skene and Henikoff 2017).

GO term enrichment analysis on co-regulated gene clusters with transiently high expression in the pre-tumor low cells revealed significant enrichment for development and differentiation-related genes (data not shown). The *de novo* DNA motif discovery analysis in the DNA sequences of the promoters of these clustered genes shows enrichment for homeodomain-containing transcription factors motif (data not shown). Thus, an untimely increase in expression of homeodomain transcription factors and their target developmental genes in the pre-tumor cells could be the event leading to their transformation into tumor cells. A recent study of human transcription factors showed homeodomain transcription factors to have higher binding affinity for methylated DNA (Yin et al., 2017). In tumor cells, the continued expression of these homeodomain transcription factors could therefore actively transcribe their target genes despite those genes having hypermethylated promoters. In conclusion, our study suggests a role for untimely expression of developmental genes in promoting the transition of wild-type cells into tumor cells, which with further characterization could potentially form the basis for novel drug targets.

## 10. References


Arabi, A., Wu, S., Ridderstråle, K., Bierhoff, H., Shiue, C., Fatyol, K., Fahlén, S., Hydbring, P., Söderberg, O., Grummt, I., et al. (2005). c-Myc associates with ribosomal DNA and activates RNA polymerase I transcription. Nat. Cell Biol. 7, 303–310.

Armitage, P., and Doll, R. (1954). The age distribution of cancer and a multi-stage theory of carcinogenesis. Br. J. Cancer 8, 1–12.

Audia, J.E., and Campbell, R.M. (2016). Histone modifications and cancer. Cold Spring Harb. Perspect. Biol. 8, a019521.

Bailey, M.H., Tokheim, C., Porta-Pardo, E., Sengupta, S., Bertrand, D., Weerasinghe, A., Colaprico, A., Wendl, M.C., Kim, J., Reardon, B., et al. (2018). Comprehensive characterization of cancer driver genes and mutations. Cell 173, 371–385.e18.

Balkwill, F.R., Capasso, M., and Hagemann, T. (2012). The tumor microenvironment at a glance. J. Cell Sci. 125, 5591–5596.

Baylin, S.B., and Jones, P.A. (2016). Epigenetic determinants of cancer. Cold Spring Harb. Perspect. Biol. 8.

Bernhart, S.H., Kretzmer, H., Holdt, L.M., Jühling, F., Ammerpohl, O., Bergmann, A.K., Northoff, B.H., Doose, G., Siebert, R., Stadler, P.F., et al. (2016). Changes of bivalent chromatin coincide with increased expression of developmental genes in cancer. Sci. Rep. 6, 37393.

Bernstein, B.E., Mikkelsen, T.S., Xie, X., Kamal, M., Huebert, D.J., Cuff, J., Fry, B., Meissner, A., Wernig, M., Plath, K., et al. (2006). A bivalent chromatin structure marks key developmental genes in embryonic stem cells. Cell 125, 315–326.

Bierhoff, H., Schmitz, K., Maass, F., Ye, J., and Grummt, I. (2010). Noncoding transcripts in sense and antisense orientation regulate the epigenetic state of ribosomal RNA genes. Cold Spring Harb. Symp. Quant. Biol. 75, 357–364.

Bogdanović, O., and Veenstra, G.J.C. (2009). DNA methylation and methyl-CpG binding proteins: developmental requirements and function. Chromosoma 118, 549–565.

Caburet, S., Conti, C., Schurra, C., Lebofsky, R., Edelstein, S.J. and Bensimon, A. (2005). Human ribosomal RNA gene arrays display a broad range of palindromic structures. Genome Research 15(8), pp. 1079–1085.

Cedar, H., and Bergman, Y. (2012). Programming of DNA methylation patterns. Annu. Rev. Biochem. 81, 97–117.

Chédin, F. (2011). The DNMT3 family of mammalian de novo DNA methyltransferases. Prog. Mol. Biol. Transl. Sci. 101, 255–285.

Croxford, J.L., Tang, M.L.F., Pan, M.F., Huang, C.W., Kamran, N., Phua, C.M.L., Chng, W.J., Ng, S.B., Raulet, D.H., and Gasser, S. (2013). ATM-dependent spontaneous regression of early Eμ-myc-induced murine B-cell leukemia depends on natural killer and T cells. Blood 121, 2512–2521.

Derenzini, M., Montanaro, L. and Trerè, D. (2017). Ribosome biogenesis and cancer. Acta Histochemica 119(3), pp. 190–197.

Derenzini, E., Rossi, A., and Treré, D. (2018). Treating hematological malignancies with drugs inhibiting ribosome biogenesis: when and why. J. Hematol. Oncol. 11, 75.

Devlin, J.R., Hannan, K.M., Hein, N., Cullinane, C., Kusnadi, E., Ng, P.Y., George, A.J., Shortt, J., Bywater, M.J., Poortinga, G., Sanij, E., Kang, J., Drygin, D., O'Brien, S., Johnstone, R.W., McArthur, G.A., Hannan, R.D. and Pearson, R.B. (2016). Combination Therapy Targeting Ribosome Biogenesis and mRNA Translation Synergistically Extends Survival in MYC-Driven Lymphoma. Cancer discovery 6(1), pp. 59–70.

Drygin, D., Lin, A., Bliesath, J., Ho, C.B., O'Brien, S.E., Proffitt, C., Omori, M., Haddach, M., Schwaebe, M.K., Siddiqui-Jain, A., et al. (2011). Targeting RNA polymerase I with an oral small molecule CX-5461 inhibits ribosomal RNA synthesis and solid tumor growth. Cancer Res. 71, 1418–1430.

Du, J., Johnson, L.M., Jacobsen, S.E., and Patel, D.J. (2015). DNA methylation pathways and their crosstalk with histone methylation. Nat. Rev. Mol. Cell Biol. 16, 519–532.

Easwaran, H.P., Schermelleh, L., Leonhardt, H., and Cardoso, M.C. (2004). Replication-independent chromatin loading of Dnmt1 during G2 and M phases. EMBO Rep. 5, 1181–1186.

Ehrlich, M. (2002). DNA methylation in cancer: too much, but also too little. Oncogene 21, 5400–5413.

Goll, M.G., and Bestor, T.H. (2005). Eukaryotic cytosine methyltransferases. Annu. Rev. Biochem. 74, 481–514.

Greaves, M. (2007). Darwinian medicine: a case for cancer. Nat. Rev. Cancer 7, 213–221.

Hanahan, D., and Weinberg, R.A. (2011). Hallmarks of cancer: the next generation. Cell 144, 646–674.

Harris, A.W., Pinkert, C.A., Crawford, M., Langdon, W.Y., Brinster, R.L., and Adams, J.M. (1988). The E mu-myc transgenic mouse. A model for high-incidence spontaneous lymphoma and leukemia of early B cells. J. Exp. Med. 167, 353–371.

Haeussler, M., Zweig, A.S., Tyner, C., Speir, M.L., Rosenbloom, K.R., Raney, B.J., Lee, C.M., Lee, B.T., Hinrichs, A.S., Gonzalez, J.N., et al. (2019). The UCSC Genome Browser database: 2019 update. Nucleic Acids Res. 47, D853–D858.

Huang, Y., and Rao, A. (2014). Connections between TET proteins and aberrant DNA modification in cancer. Trends Genet. 30, 464–474.

Knudson, A.G. (1971). Mutation and cancer: statistical study of retinoblastoma. Proc Natl Acad Sci USA 68, 820–823.

Kulis, M., and Esteller, M. (2010). DNA methylation and cancer. Adv. Genet. 70, 27–56.

Lefebure, M., Tothill, R.W., Kruse, E., Hawkins, E.D., Shortt, J., Matthews, G.M., Gregory, G.P., Martin, B.P., Kelly, M.J., Todorovski, I., et al. (2017). Genomic characterisation of Eμ-Myc mouse lymphomas identifies Bcor as a Myc co-operative tumour-suppressor gene. Nat. Commun. 8, 14581.

Levitin, H.M., Yuan, J., and Sims, P.A. (2018). Single-Cell Transcriptomic Analysis of Tumor Heterogeneity. Trends Cancer 4, 264–268.

Lin, C.-P., and He, L. (2017). Noncoding rnas in cancer development. Annu. Rev. Cancer Biol. 1, 163–184.

Luger, K., Mäder, A.W., Richmond, R.K., Sargent, D.F., and Richmond, T.J. (1997). Crystal structure of the nucleosome core particle at 2.8 A resolution. Nature 389, 251–260.

Meller, V.H., Joshi, S.S., and Deshpande, N. (2015). Modulation of chromatin by noncoding RNA. Annu. Rev. Genet. 49, 673–695.

Mikkelsen, T.S., Ku, M., Jaffe, D.B., Issac, B., Lieberman, E., Giannoukos, G., Alvarez, P., Brockman, W., Kim, T.-K., Koche, R.P., et al. (2007). Genome-wide maps of chromatin state in pluripotent and lineage-committed cells. Nature 448, 553–560.

Mullineux, S.-T., and Lafontaine, D.L.J. (2012). Mapping the cleavage sites on mammalian pre-rRNAs: where do we stand? Biochimie 94, 1521–1532.

Neri, F., Rapelli, S., Krepelova, A., Incarnato, D., Parlato, C., Basile, G., Maldotti, M., Anselmi, F., and Oliviero, S. (2017). Intragenic DNA methylation prevents spurious transcription initiation. Nature 543, 72–77.

Ngo, V., Chen, Z., Zhang, K., Whitaker, J.W., Wang, M., and Wang, W. (2019). Epigenomic analysis reveals DNA motifs regulating histone modifications in human and mouse. Proc Natl Acad Sci USA.

O'Sullivan AC, Sullivan GJ, McStay B. UBF binding in vivo is not restricted to regulatory sequences within the vertebrate ribosomal DNA repeat. Mol. Cell. Biol. 2002; 22: 657–668.

Pelletier, J., Thomas, G., and Volarević, S. (2018). Ribosome biogenesis in cancer: new players and therapeutic avenues. Nat. Rev. Cancer 18, 51–63.

Poole, C.J., Zheng, W., Lodh, A., Yevtodiyenko, A., Liefwalker, D., Li, H., Felsher, D.W. and van Riggelen, J. (2017). DNMT3B overexpression contributes to aberrant DNA methylation and MYC-driven tumor maintenance in T-ALL and Burkitt's lymphoma. Oncotarget 8(44), pp. 76898–76920.

Reik, W. (2007). Stability and flexibility of epigenetic gene regulation in mammalian development. Nature 447, 425–432.

Rodriguez, J., Muñoz, M., Vives, L., Frangou, C.G., Groudine, M., and Peinado, M.A. (2008). Bivalent domains enforce transcriptional memory of DNA methylated genes in cancer cells. Proc Natl Acad Sci USA 105, 19809–19814.

Salim, D., and Gerton, J.L. (2019). Ribosomal DNA instability and genome adaptability. Chromosome Res. 27, 73–87.

Santoro, R., and Grummt, I. (2001). Molecular mechanisms mediating methylation-dependent silencing of ribosomal gene transcription. Mol. Cell 8, 719–725.

Santoro, R. and Grummt, I. (2005). Epigenetic mechanism of rRNA gene silencing: temporal order of NoRC-mediated histone modification, chromatin remodeling, and DNA methylation. Molecular and Cellular Biology 25(7), pp. 2539–2546.

Schlosser, I., Hölzel, M., Mürnseer, M., Burtscher, H., Weidle, U.H., and Eick, D. (2003). A role for c-Myc in the regulation of ribosomal RNA processing. Nucleic Acids Res. 31, 6148–6156.

Schmitz, K.-M., Mayer, C., Postepska, A. and Grummt, I. (2010). Interaction of noncoding RNA with the rDNA promoter mediates recruitment of DNMT3b and silencing of rRNA genes. Genes & Development 24(20), pp. 2264–2269.

Sharifi, S., and Bierhoff, H. (2018). Regulation of RNA polymerase I transcription in development, disease, and aging. Annu. Rev. Biochem. 87, 51–73.

Skene, P.J. and Henikoff, S. (2017). An efficient targeted nuclease strategy for high-resolution mapping of DNA binding sites. eLife 6.

Sproul, D., and Meehan, R.R. (2013). Genomic insights into cancer-associated aberrant CpG island hypermethylation. Brief. Funct. Genomics 12, 174–190.

Srivastava, R., Srivastava, R., and Ahn, S.H. (2016). The epigenetic pathways to ribosomal DNA silencing. Microbiol. Mol. Biol. Rev. 80, 545–563.

Strohner, R., Nemeth, A., Jansa, P., Hofmann-Rohrer, U., Santoro, R., Längst, G., and Grummt, I. (2001). NoRC--a novel member of mammalian ISWI-containing chromatin remodeling machines. EMBO J. 20, 4892–4900.

Suganuma, T., and Workman, J.L. (2011). Signals and combinatorial functions of histone modifications. Annu. Rev. Biochem. 80, 473–499. Dnmt2 is required for accurate polypeptide synthesis during haematopoiesis. EMBO J. 34, 2350–2362.

Veland, N., Lu, Y., Hardikar, S., Gaddis, S., Zeng, Y., Liu, B., Estecio, M.R., Takata, Y., Lin, K., Tomida, M.W., et al. (2019). DNMT3L facilitates DNA methylation partly by maintaining DNMT3A stability in mouse embryonic stem cells. Nucleic Acids Res. 47, 152–167.

Weber, M., Hellmann, I., Stadler, M.B., Ramos, L., Pääbo, S., Rebhan, M., and Schübeler, D. (2007). Distribution, silencing potential and evolutionary impact of promoter DNA methylation in the human genome. Nat. Genet. 39, 457–466.

Wellenstein, M.D., and de Visser, K.E. (2018). Cancer-Cell-Intrinsic Mechanisms Shaping the Tumor Immune Landscape. Immunity 48, 399–416.

Wong, K.M., Hudson, T.J., and McPherson, J.D. (2011). Unraveling the genetics of cancer: genome sequencing and beyond. Annu. Rev. Genomics Hum. Genet. 12, 407–430.

Wu, H., and Zhang, Y. (2011). Mechanisms and functions of Tet protein-mediated 5-methylcytosine oxidation. Genes Dev. 25, 2436–2452.

Yin, Y., Morgunova, E., Jolma, A., Kaasinen, E., Sahu, B., Khund-Sayeed, S., Das, P.K., Kivioja, T., Dave, K., Zhong, F., et al. (2017). Impact of cytosine methylation on DNA binding specificities of human transcription factors. Science 356.

Yoder, J.A., Walsh, C.P., and Bestor, T.H. (1997). Cytosine methylation and the ecology of intragenomic parasites. Trends Genet. 13, 335–340.

Yuan, X., Zhao, J., Zentgraf, H., Hoffmann-Rohrer, U., and Grummt, I. (2002). Multiple interactions between RNA polymerase I, TIF-IA and TAF(I) subunits regulate preinitiation complex assembly at the ribosomal gene promoter. EMBO Rep. 3, 1082–1087.

Zhang, W., and Xu, J. (2017). DNA methyltransferases and their roles in tumorigenesis. Biomark. Res. 5, 1.

Zhao, Y., and Garcia, B.A. (2015). Comprehensive catalog of currently documented histone modifications. Cold Spring Harb. Perspect. Biol. 7, a025064.